CrossMark
← click for updates

Flow of DNA in micro/nanofluidics: From fundamentals to applications

Lea Rems,[1] Durgesh Kawale,[1] L. James Lee,[2] and Pouyan E. Boukany[1,a)]

[1]*Department of Chemical Engineering, Delft University of Technology, Delft 2629HZ, The Netherlands*
[2]*William G. Lowrie Department of Chemical and Biomolecular Engineering, The Ohio State University, Columbus, Ohio 43210, USA*

Thanks to direct observation and manipulation of DNA in micro/nanofluidic devices, we are now able to elucidate the relationship between the polymer microstructure and its rheological properties, as well as to design new single-molecule platforms for biophysics and biomedicine. This allows exploration of many new mechanisms and phenomena, which were previously unachievable with conventional methods such as bulk rheometry tests. For instance, the field of polymer rheology is at a turning point to relate the complex molecular conformations to the nonlinear viscoelasticity of polymeric fluids (such as coil–stretch transition, shear thinning, and stress overshoot in startup shear). In addition, nanofluidic devices provided a starting point for manipulating single DNA molecules by applying basic principles of polymer physics, which is highly relevant to numerous processes in biosciences. In this article, we review recent progress regarding the flow and deformation of DNA in micro/nanofluidic systems from both fundamental and application perspectives. We particularly focus on advances in the understanding of polymer rheology and identify the emerging research trends and challenges, especially with respect to future applications of nanofluidics in the biomedical field. *Published by AIP Publishing.* [http://dx.doi.org/10.1063/1.4958719]

I. INTRODUCTION

Understanding the deformation and flow of (bio)polymers, such as DNA, is a critical challenge in life sciences as well as in polymer science and engineering.[1] Beyond the DNA's biological relevance as the carrier of the genetic information in all forms of life, the DNA can also be employed as a model polymer for experiments relevant to fundamental studies on polymer physics. Compared with synthetic model polymers, DNA has several advantages including ease of fluorescent labeling and narrow size distribution at a given number of DNA base pairs (bp ~ 0.34 nm). In addition, DNA can be prepared in a variety of sizes ranging from just few base pairs to hundreds of thousands of base pairs via gene synthesis and genetic engineering techniques.[2,3] Fluorescently labeled DNA with typically used contour length L of several tens of micrometers can be visualized under a common fluorescence microscope while still being classified as a (semi-)flexible chain under physiological conditions, since the DNA's persistence length P is only about 50 nm.[4] Furthermore, micro/nanofluidics is nowadays an established technology, which offers unique features to explore and examine biological and complex fluids under controlled and reproducible conditions.[5,6] Different fluidic geometries with spatial scales from nanometers to centimeters can be fabricated by soft lithography and etching techniques.[7–9] Combination of micro/nanofluidics and DNA visualization has allowed scientists to test polymer theories directly against experiments at the single-molecule level, which presents an important step for advancements in both polymer rheology and genomic sciences.

---

a)Author to whom correspondence should be addressed. Electronic mail: P.E.Boukany@tudelft.nl.

In contrast to Newtonian fluids, polymeric fluids exhibit complex flow behaviors such as shear thinning, rod climbing, transient stress-overshoot during shear, and flow instabilities, which are related to flow-induced changes in polymer molecular conformations at very high deformation rates. However, the exact molecular picture behind many of these complex flow responses is not well-understood and is still under debate.[10,11] This limits the design, control, and optimization of the technological processes related to polymer products.[12] In order to overcome the technological limitations, it is essential to develop new methods that can link the macroscopic flow responses with the molecular conformation of polymer molecules in the flow.

Traditionally, polymer rheologists focused on measuring the macroscopic flow responses using "bulk" experimental methods including rotational rheometry, light scattering, and birefringence.[13,14] In such bulk measurements, the rheological properties of polymers are averaged over an ensemble of many molecules. In the past two decades, the approach of analyzing the rheological response has been changed by utilizing newly developed tools such as microfluidics-based rheometers[15] coupled with advanced single-molecule techniques.[16,17] In particular, direct observation of individual DNA molecules during flow in microfluidic channels provided a fresh insight into the nature of the rheological responses of polymeric fluids by describing the flow properties on the single-molecule level.[2,16,18,19] For instance, single-molecule experiments have directly shown the details of how coiled DNA molecules become significantly stretched when the hydrodynamic flow rate is sufficiently fast, which revealed a complex transition from the equilibrium (coiled) to the non-equilibrium (un-coiled) conformation.[20,21]

Hydrodynamic flow is, however, not the only way to induce strong deformation of the DNA chain. Polymer scientists have recognized that similar or greater level of deformation could be achieved by confining DNA molecules in nanoscale geometries. One of the main motivations for studying the physics of confined DNA comes from genomic sciences, since the ability to uncoil and stretch the DNA by confinement allows for easier and more accurate reading of genomic information.[22–25] To this end, the advancement of nanofabrication technologies[26] has provided unprecedented possibilities to study and manipulate DNA molecules in confined nanofluidic environments. Over the past decade, the use of nanofluidics for DNA manipulation has received enormous attention for applications such as genome mapping,[27–29] and DNA sequencing,[25,30,31] as well as for DNA sorting/separation,[32–34] and DNA transfer into live cells.[35]

In this spirit, the present review article overviews the use of microfluidic and nanofluidic systems to visualize, study, and manipulate DNA molecules. The first part of the article (Section II) focuses on how the field of polymer rheology has benefitted from flow studies of DNA inside microfluidic systems by relating the complex conformation of DNA molecules to their flow responses. The second part of the article (Section III) aims to explore DNA deformation and dynamics under confinement and discusses applications of nanofluidic devices for biomedical applications.

II. DNA FLOW IN MICROFLUIDICS

Different types of flow fields such as shear, extension, and compression can co-exist during polymer processing operations. Understanding the physics of such viscoelastic flows can be extremely challenging, because of the competition between various forces such as inertia, viscosity, and elasticity of polymeric materials. The development of microfluidics stimulated the interest in investigating the rheological response of polymeric fluids in microfluidic devices, because the latter offer an easy control over inertial and elastic forces in experiments.

In Secs. II A–II E, we first introduce the dimensionless groups, which are later used in the article to characterize the dominant forces governing a given flow behavior (Section II A). We then continue with a brief discussion on the general use of DNA molecules for visualization of the polymer conformations within the flow field (Section II B). Finally, we describe in greater detail how a stained DNA molecule has been used as a model polymer to study the relaxation of stretched (deformed) polymers, and polymer molecular conformations in extensional, shear, and other industrially relevant flows at high Weissenberg number (Sections II C–II E). These

studies have been helpful in understanding the rheological properties of polymer solutions by validating basic polymer theories at the single-molecule level.

A. Dimensionless groups

Dimensional analysis is a powerful tool to identify the dominant forces in complex flows of polymeric materials.[36] Four dimensionless groups are highly relevant to rheological studies of polymers: the Reynolds number (Re), the Weissenberg number (Wi), the Deborah number (De), and the elasticity number (El).

The definition of the Reynolds number is given as $Re = \rho V l / \eta$, where ρ is the fluid density, V is the average velocity, l is a characteristic length scale, and η is the fluid viscosity. The Weissenberg number is defined for shear flow as $Wi = \dot{\gamma}\tau$, for channel flow as $Wi = (V/l)\tau$, and for extensional flow as $Wi = \dot{\varepsilon}\tau$, where $\dot{\gamma}$ is the shear strain rate, $\dot{\varepsilon}$ is the extensional strain rate, and τ is the longest relaxation time.

The Deborah number was originally defined as $De = \tau/t_{obs}$, where t_{obs} is the observation time during transient deformation.[37,38] There has been a lot of confusion about the intended usage of Wi and De numbers in order to generalize the findings from a particular rheological problem. In some literature, different definition of De has been proposed, by altering the time of observation to either the process time or the residence time in a given flow field. Therefore, De has been also defined as the ratio of the sample's characteristic relaxation time to the characteristic flow rate, i.e., $De = \dot{\varepsilon}\tau$ or $De = (V/l)\tau$. To avoid confusion in this review, we will consider the original definition of De.[38] According to the original definition, the observation time can be infinite resulting in $De \sim 0$ in steady flows (such as steady simple shear and extension). Hence, we will retain Wi to characterize the ratio between the polymer relaxation time and convective time scales.[39]

Finally, the elasticity number presents the ratio between the elastic and inertial forces and is defined as $El = Wi/Re$. Elasticity number is independent of the fluid kinematics as this number is independent of fluid velocity. To summarize the guidelines on how to use these numbers, see Table I.

The key advantage of microfluidic devices is that one can achieve high Wi at low Re, which allows us to reach higher El flows compared to conventional fluidic devices (see Table I). A wide variety of flow instabilities, such as vortex formation, shear banding, wall slip, and elastic turbulence, may occur in microfluidic devices, depending on the value of these dimensionless numbers. For example, Rodd *et al.*[40] could explore new regimes in contraction flows of polymer solutions, as shown in Fig. 1. This microfluidic platform provided a unique opportunity for them to study the effect of elasticity on vortex instability in polymer solutions at high Wi and low Re.

TABLE I. Relevant dimensionless numbers used in this review.

			Achievable range	
	Physical interpretation	Definition	Conventional fluidic devices	Microfluidic devices
Re	$\dfrac{Inertial\,force}{Viscous\,force}$	$\dfrac{\rho V l}{\eta}$	$\sim 10^{-2}$–10^{4} [a]	$\sim 10^{-5}$–10 [b]
De	$\dfrac{Elastic\,force}{Time\,of\,observation}$	$\dfrac{\tau}{t_{obs}}$	~ 0–∞	~ 0–∞
Wi	$\dfrac{Elastic\,force}{Viscous\,force}$	Shear flow: $\dot{\gamma}\tau$ Extensional flow: $\dot{\varepsilon}\tau$ Channel flow: $(V/l)\tau$	$\sim 10^{-7}$–10^{2}	$\sim 10^{-4}$–10^{5} [b,c]
El	$\dfrac{Elastic\,force}{Inertial\,force}$	$\dfrac{Wi}{Re}$	$\sim 10^{-5}$–10^{-2}	~ 10–10^{4} [b]

[a]Re can be even higher than 10^4, but the higher limit depends on how much pressure the system can handle.
[b]Assuming that a typical PDMS-based microfluidic device would be delaminated at pressure higher than 1 bar.
[c]Assuming maximum $\dot{\gamma} = 1000\,\text{s}^{-1}$ and $\tau = 100\,\text{s}$.
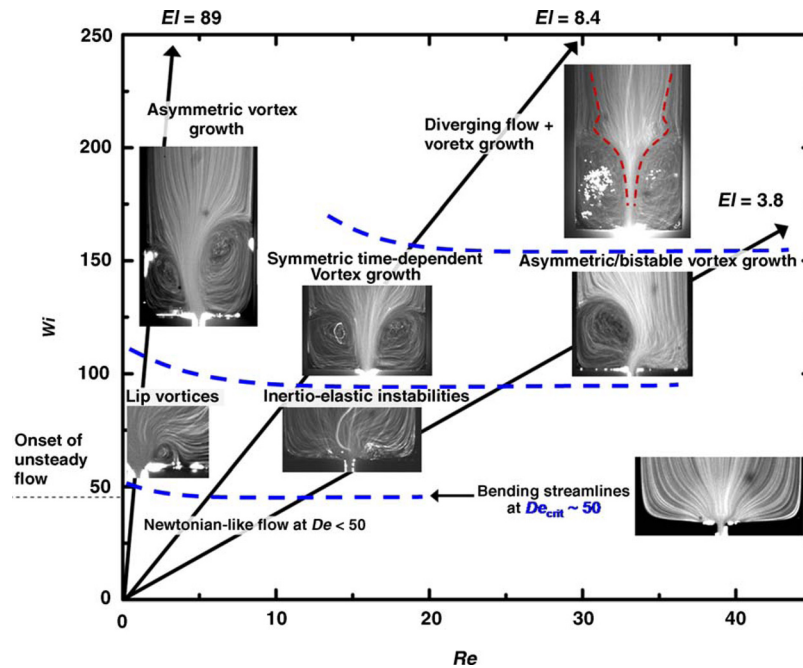
FIG. 1. Microfluidic devices explored new regimes in *Wi–Re* space for polymeric fluids flowing through contraction geometries. Reproduced with permission from Rodd *et al.*, J. Non-Newton. Fluid Mech. **129**, 1 (2005). Copyright 2005 Elsevier.[40]

B. DNA as a model polymer for visualization

Flows of polymer solutions were traditionally visualized and investigated by integrating (micro)fluidic geometries with optical/confocal microscopy and using velocimetry techniques. These velocimetry techniques mainly include the Particle Tracking Velocimetry (PTV), the Particle Streak Velocimetry (PSV), and the Particle Image Velocimetry (PIV), which are based on imaging the position of micro-tracer particles suspended in the polymer solution.[17,41–43] These effective methods could determine the onset of flow instability in polymer solutions at high *Wi* (or high *El*). However, they could not provide sufficient information on the flow-induced polymer conformation.[43]

Using DNA as a molecular tracer has opened new avenues for polymer rheologists to study the polymer conformation in viscoelastic flows. DNA molecules can be stained with a fluorescent dye, such as YOYO-1 or TOTO-1,[44] which makes them visible under a fluorescence microscope when illuminated at the excitation wavelength of the dye. In the first attempts to visualize the conformation of an individual DNA molecule within the flow field, tiny amounts of fluorescently stained DNA molecules as test chains were dispersed in a solution of unstained DNA molecules (background chains). Using this approach, the stained DNA molecules and their conformations could be visualized as representative of the unstained DNA molecules. These fundamental studies of DNA dynamics were carried out in simple fluidic geometries to produce extensional or shear flow. Later on, complex geometries were also studied by introducing contraction geometries and integrating obstacles inside microfluidic devices.[45–47] Moreover, stained DNA molecules were also used as molecules probes in a solution of (unstained) synthetic polymers such as polyethylene oxide (with similar contour length *L*) in order to measure polymer conformations and velocity fields during flow.[48]

Recently, synthetic polymers including polyacrylamide and poly(methyl methacrylate) have also been labeled with a fluorescent dye.[49–51] However, the protocol of attaching fluorescent probes to synthetic polymers is tediously elaborate and challenging for routine applications in rheology testing laboratories. Ease of staining and manipulation is perhaps the greatest advantage of DNA over synthetic polymers. Therefore, DNA molecules are still being employed as popular fluorescent probes to study polymeric conformations within the flow field.

Nevertheless, to obtain quantitative information about the DNA chain extension in strong flows, one must be aware that the staining increases the contour length of DNA. The increase in contour length is a function of the ratio between the number of added dye molecules per DNA base pairs, and about 38% increase in contour length has been reported for 1 YOYO-1 per 4 DNA base pairs.[52,53] Furthermore, DNA is a negatively charged polyelectrolyte (similar to poly(sodium styrene sulfonate), polyacrylic acid, etc.). Therefore, its persistence length P is a function of the ionic strength in the aqueous solution. In the limit of high salt concentration (>10 mM), DNA is a semi-flexible molecule with $P \sim 50$ nm. When reducing the salt concentration, DNA significantly stiffens. At 0.1 mM salt, the reported P of DNA is around 350 nm.[54] Consequently, most flow studies based on DNA visualization should be performed in buffer solutions containing sufficient amount of salt to decrease the stiffness of the DNA as well as to neutralize its charges.

C. Relaxation of stretched DNA: Zimm and Reptation theory meet experiments

The relaxation of stretched polymers is of fundamental importance in describing the visco-elastic properties of polymeric fluids.[55] Stress relaxation measurement is generally carried out using bulk rheometry. In this test, a polymer sample is suddenly deformed by a fixed amount of deformation (called step strain), and the resulting stress decay is monitored over time when the deformation is stopped (after step shear). In this classical approach, the relaxation response of single polymers needs to be interpreted from indirect measurements averaged over an ensemble of polymer chains.

Polymer experimentalists have attempted to understand the relaxation behavior of an isolated polymer chain upon cessation of the flow (or deformation) to validate theoretical predictions using single-molecule DNA measurements. These relaxation methods have been applied to both isolated polymers[56] and concentrated polymer solutions,[57] where the interaction between the test chain and the surrounding chains becomes important.

Zimm model[58] is one of the most powerful theories of polymer dynamics, which has been successfully applied in dilute polymer solutions. This model treats the polymer chain as a string of beads connected by Hookean springs, where the beads hydrodyamically interact with the solvent. Based on this model, the relaxation time of an isolated polymer scales as $\tau \sim M^{3\upsilon} \sim L^{3\upsilon}$, where M is the molecular weight of the polymer, L is the polymer contour length, and 3υ is the scaling exponent. Within Zimm model,[58] the value of 3υ is 1.5 and 1.8 for theta and good solvents, respectively. Until the advent of using DNA as a model polymer, this scaling law was tested by indirect methods (intrinsic viscosity,[59] dynamic light scattering,[60] and birefringence[61]) giving a value ranging from 1.5 to 1.65. In order to validate the scaling law directly, Perkins *et al.*[56] stretched single isolated DNA molecules in a strong flow (at $Wi > 1.0$), and visualized the relaxation process under the microscope after stopping the flow (see Fig. 2(a)). In their experiments, a DNA molecule was tethered by one end to a microbead, which was held still by optical tweezers, and the molecule was stretched by laterally moving the microscope stage. They found that the relaxation time scales as $\tau \sim L^{1.65}$, in qualitative agreement with predictions from the Zimm model. Although the experimental value is close to the theoretical value, it is debatable whether the DNA molecules used in their experiments can be considered as a "universal" polymer model, for which the Zimm's scaling law would be directly applicable. According to de Gennes,[62] a polymer approaches universality when the polymer is sufficiently long, such that its behavior is independent of its chemical structure. In the case of the double-stranded DNA, Tree *et al.*[63] numerically showed that universality occurs only for ultra-long chains ($\sim$1 Mbp, i.e., at least few 100 μm long), whereas typically used DNA molecules in experiments ($\sim$100 kbp) are somewhere in the middle of the transition to long-chain behavior. Consequently, the DNA molecules used by Perkins *et al.*[56] (4–43 μm long) were probably somewhere in a transition regime of the Zimm's scaling exponent.

Later, DNA molecules have been successfully used to understand the rheological behavior of concentrated polymer solutions. Examining the molecular dynamics of concentrated polymer solutions is a challenging task, because of high degree of interaction among polymer chains.
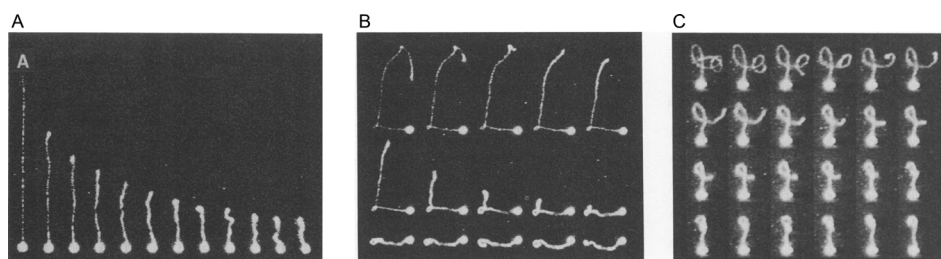
FIG. 2. Relaxation responses of individual DNA molecules in (a) dilute and ((b) and (c)) concentrated (entangled) solutions. (a) Relaxation of a single DNA molecule, where the DNA is stretched around 40 μm in a flow and its relaxation is measured after cessation of the flow. Subsequent images are separated by 4.5 s. Reproduced with permission from Perkins *et al.*, Science **264**, 822 (1994). Copyright 1994 The American Association for the Advancement of Science.[56] ((b) and (c)) Series of images showing reptating tube-like DNA motion in a concentration solution of DNA molecules ((a): 12 molecules/μm^3, (b): 7 molecules/μm^3). The fluorescently labeled DNA was tethered to a fluorescent microbead, which was controlled by optical tweezers. The sequence of images starts at time 0 s (top row, left) after stopping the movement of the microbead. In (b) the image sequence is shown up to 128 s (bottom row, right). Note that the topological constraints imposed by the background polymers persisted in excess of 120 s, as shown by the persistence of the small loop of DNA near the microbead. In (c) the images are separated by 1.5 s. Reproduced with permission from Perkins *et al.*, Science **264**, 819 (1994). Copyright 1994 The American Association for the Advancement of Science.[57]

Polymers in concentrated solutions ($C > C^*$, where C^* is the overlap concentration), are entangled with each other like cooked spaghetti. To theoretically address concentrated polymer solutions, de Gennes, Doi, and Edwards[18,64] proposed an elegant concept of reptation. In this model, an entangled polymer is assumed to be confined inside an imaginary tube through which it can move in a snake-like fashion. When the polymer traverses through this imaginary tube, the tube deforms and exerts strain on the surrounding polymers. The theoretical assumptions of the tube-like motion were experimentally confirmed on the single-polymer level by Perkins *et al.*[57] The experiment was performed by visualizing a single fluorescently labelled DNA molecule (test chain) in an entangled solution of unlabeled DNA. The test chain was attached by one end to a microbead and pulled through the entangled solution by optical tweezers. As the test chain was pulled, it closely followed the path of the microbead, allowing for various conformations to be "drawn" with the test chain, such as kinks and loops (Figs. 2(b) and 2(c)). After releasing the stress, the test chain slowly relaxed following the drawn path in reverse. In small loops, this tube-like motion persisted for over 2 min. Using a similar protocol, Smith *et al.*[65] further corroborated the theoretical predictions from the reptation model by measuring the diffusion coefficient of entangled DNA molecules. The model predicts that the diffusion coefficient scales with L^{-2}. The experimentally determined scaling exponent of -1.8 ± 0.1 was indeed close to the theoretical.

Teixeira *et al.*[66] employed a step shear test to investigate the relaxation behavior of entangled (concentrated) DNA solutions by direct visualization of individual DNA molecules. Two distinct relaxation time scales were found. Initially, DNA solutions relaxed very fast, because chain retraction occurred almost instantaneously. Later, reptation mechanism started to take over as the slower relaxation process. In addition, they showed that the slower relaxation time scaled with concentration as $\tau_{slow} \sim C^{3.3}$ ($C > C^*$). The reported exponent is higher than predicted value by pure reptation mechanism, which might originate from the effect of constraint release and contour length fluctuations on the reptative process.

Recently, Hsiao *et al.*[67] investigated the relaxation response of individual polymers in semi-dilute solutions ($C \sim C^*$). In this experiment, the polymer solution was flowed into a microfluidic cross-slot channel at high Wi, followed by sudden cessation of the fluid flow. They also found a power-law scaling $\tau \sim (C/C^*)^{0.48}$, which was in good agreement with bulk rheological tests.

Furthermore, Li *et al.*[68] studied the effect of chain topology (linear or circular chains) on the relaxation process of single DNA molecules by cessation of elongational flow. They found that circular DNA relaxed faster and exhibited a lower scaling exponent ($3\upsilon \sim 1.4$) compared to linear DNA ($3\upsilon \sim 1.7$). They speculated that lower exponent might be an evidence of the

absence of excluded volume effects in circular DNA. It is expected that circular DNA is effectively ($\sim$50%) shorter than linear DNA with same molecular weight. Therefore, excluded volume is seen to be less important in circular DNA compared with linear DNA.

With respect to the influence of the chain topology on the polymer relaxation dynamics, an upcoming area of research is the effect of DNA branching, wherein one of the challenges is to synthesize branched DNA molecules.[69,70]

D. Dynamics of individual DNA molecules in fluid flow

The field of polymer rheology is concerned with the description of the flow behavior of polymeric fluids in strong flow. In this section, we focus on single-DNA rheology, which provided direct link to bulk viscoelasticity of polymers under controlled fluidic flows such as extension, shear, and mixed flows relevant to industrial operations. Initial single-molecule measurements in fluid flow were performed mainly on dilute polymer solutions. The assumption of dilute solution is that the intermolecular interactions are negligible, and the polymer is treated as a single isolated chain. Later, fluorescently stained DNA molecules were added in a background of unstained chains enabling to test semi-dilute and concentrated polymer solutions in the flow.[54,66] Understanding the flow behavior of concentrated polymer solutions and entangled melts is very important in numerous industrial process such as injection molding, inkjet printing, coating, and fiber-spinning, because most of polymer solutions and melts that have been employed in industry would be processed in the entangled state.[12] Subsections II D 1–II D 4 are organized to highlight the single-DNA measurements in different flow conditions (extensional flow, shear, contraction, and random flow) from dilute, semi-dilute to entangled DNA solutions.

1. Extensional flow: Coil–stretch transition meets experiment

In 1974, de Gennes[71] predicted that a dilute polymer solution would exhibit an instantaneous coil–stretch transition in strong flows, when the flow rate exceeds a certain critical value of Wi. Later, theoretical calculation from the generalized Zimm model and numerical calculation by Larson and Magda[72] showed that the onset of polymer stretching (coil–stretch transition) occurs at a critical strain rate, $\dot{\varepsilon}_c \sim 0.5/\tau$, where τ is the longest relaxation time. For $\dot{\varepsilon} < \dot{\varepsilon}_c$ (that is at $Wi < 0.5$), the polymer molecules are in the coiled state.

Chu's group at Stanford realized that single DNA measurements combined with a controlled microfluidic geometry could be used to experimentally test the above theoretical predictions.[20,73,74] Perkins *et al.*[20] employed a cross-slot microfluidic cell to directly visualize the conformation of DNA molecules in extensional flows. They observed an existence of a distribution of transient molecular conformations through the coil–stretch transition at a given flow rate (or Wi). The polymer molecules could be found in five main types of conformations: dumbbell, half-dumbbell, folded, kinked, or coiled (Fig. 3(a) shows the optical micrograph of these conformations). At $Wi = 3.35$, the first three types of conformations including the dumbbell, half-dumbbell, and folded were dominant. In a follow-up study, Smith and Chu[73] showed that at $Wi > 10$, many more molecules became kinked or folded, with their fraction reaching an asymptotic value of about one-third. On average, folded molecules stretched the slowest, whereas kinked molecules stretched the fastest. Figs. 3(b) and 3(c) display the progression of the level of extension with time in individual DNA molecules at $Wi = 2.0$ and $Wi = 48$, respectively. Eventually, the molecules in these different transient conformations approached an asymptotic steady-state conformation, corresponding to a nearly fully stretched straight line ($>$75% of the DNA contour length). These data confirmed that for $Wi < 0.4$, there was no stretching, and all of the molecules were coils. In addition, the ensemble average extension of the chains increased with the imposed Wi (cf. Figs. 3(b) and 3(c)). The experimentally observed transient molecular conformations could also be predicted by Brownian dynamics simulations conducted by Larson *et al.*[75] These transient conformations indicate that the coil–stretch transition proceeds in a dynamic fashion, rather than instantaneously. It further shows that polymer molecules demonstrate "individualism" in their dynamics, rather than a collective and simultaneous
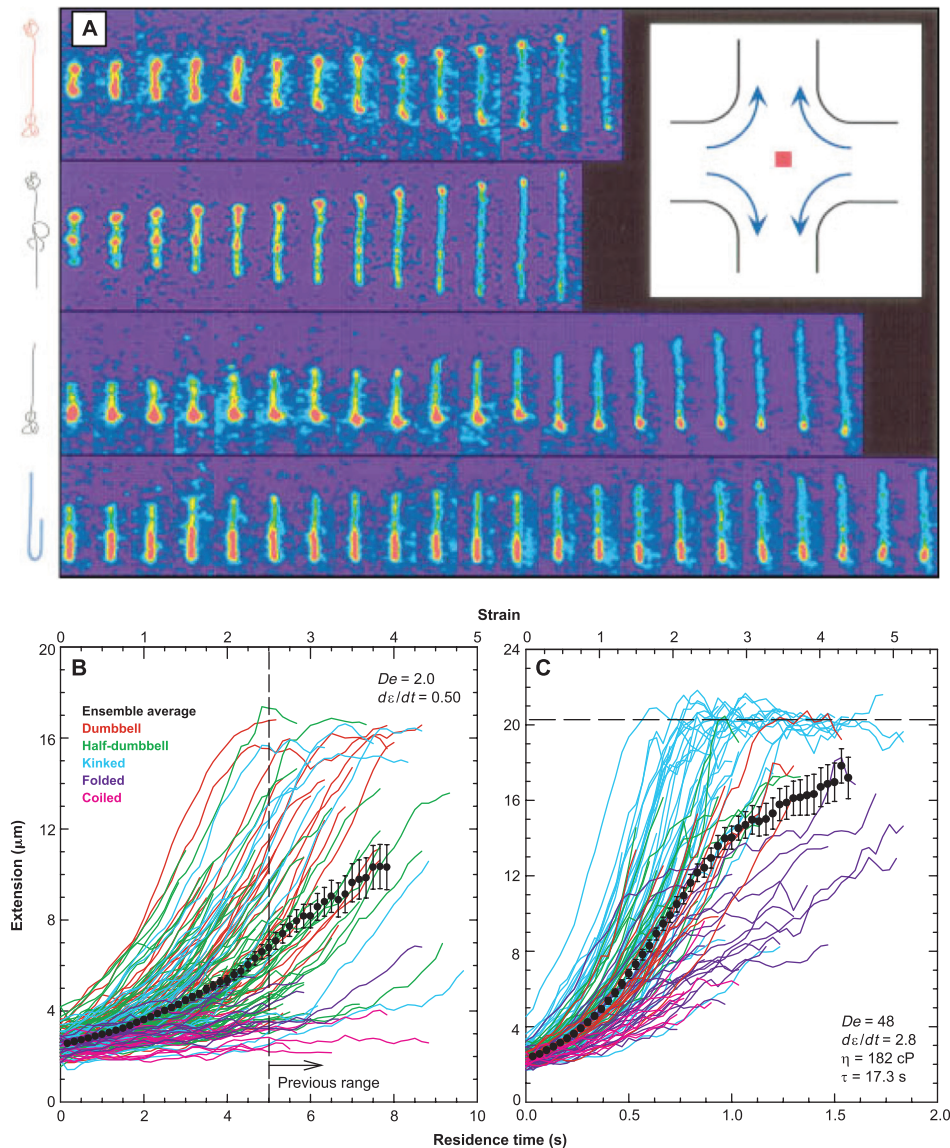
FIG. 3. (a) The dumbbell, kinked, half-dumbbell, and folded DNA conformations in extensional flow field at $Wi = 3.4$. Images are spaced at 0.13 s. Molecular extension of the last molecule in the first row is 13.9 μm. Reproduced with permission from Perkins *et al.*, Science **276**, 2016 (1997). Copyright 1997 The American Association for the Advancement of Science.[20] ((b) and (c)) Time course of the DNA extension extracted from individual DNA molecules under the same flow conditions; (b) $Wi = 2$, (c) $Wi = 48$. The molecules were categorized with respect to their transient molecular conformations (shown in (a)), as indicated by the colors of the solid lines. The solid black points represent the ensemble average extension, which increases with Wi (cf. (b) and (c)). Note that we used Wi number in the figure caption to refer to De number indicated in the figure, following the discussion given in Section II A. Reproduced with permission from D. E. Smith and S. Chu, Science **281**, 1335 (1998). Copyright 1998 The American Association for the Advancement of Science.[73]

unwinding beyond $\dot{\varepsilon}_c$. The origins of the molecular individualism are apparently governed by the details of the random initial molecular configuration of the polymer coil.[76]

de Gennes[71] also theoretically predicted that the coil–stretch transition might be associated with a strong hysteresis in molecular conformations. The existence of the hysteresis was then experimentally confirmed by Schroeder *el al.*,[74] when employing a similar cross-slot microfluidic cell to stretch very long DNA (with L from 1.3 to 1.7 mm). They showed that within a narrow range of Wi, the conformation of the molecules was either coiled or highly stretched, depending on the deformation history of the DNA.

Recently, Hsiao et al.[67] investigated the coil–stretch transition for semi-dilute DNA solution in elongational flow. They observed a milder coil–stretch transition for semi-dilute DNA solutions (when $C \sim C^*$) compared with dilute DNA solution. A possible explanation is that this critical Wi might be concentration dependent, due to either inter-chain interactions among polymers or flow-induced entanglements in strong flows.

Finally, Li et al.[68] demonstrated that circular polymers could also display a coil–stretch transition in elongational flow. However, they have found that circular polymers need higher Wi to stretch and exhibit less diverse molecular individualism during the transient stretching process compared to linear polymers. They speculated that the delay of stretching and less diverse molecular individualism during transient extension might originate from more compact structure of circular polymers and lower diversity of initial states available in circular chains, respectively, compared with linear chains.

2. Dynamics of DNA in shear flow

a. Dilute and semi-dilute solutions. After studying the coil–stretch transition in elongational flow, Chu's group investigated the nature of coil–stretch transition in steady shear flow. Shear flow can also be considered as a superposition of a purely elongational and a purely rotational flow. de Gennes[71] had proposed that the presence of the rotational component in shear flows above $Wi > 0.5$ would drive the polymer molecules to a constantly fluctuating first-order coil–stretch transition. Smith et al.[77] experimentally demonstrated that the average DNA extension in steady shear flow indeed does not display a sharp coil–stretch transition. Instead, large fluctuations in polymer extension were observed that were consistent with repeating end-to-end tumbling of the molecule. The conformation of a given molecule continuously changed, and at different times, dumbbell, half-dumbbell, kinked, and folded shapes were observed, similar to those in extensional flow (Fig. 3(a)). The ensemble average extension of the molecules in shear flow also increased with Wi. However, the increase in the average extension with Wi was much more gradual than in extensional flow, and the highest average extension reached only about 40%–50% of the DNA contour length for Wi higher than ~ 40. Schroeder et al.[78] then demonstrated that the fluctuations in the polymer extension can be attributed to periodic cycling motion of the polymer as shown in Fig. 4. Above $Wi > 0.5$, the flow is strong enough to overcome the entropic elasticity of the coiled chain and stretch the molecule along the flow direction. As the polymer molecule extends in the direction perpendicular to the shearing flow plane, it is stretched due to hydrodynamic drag until it reaches a maximum stretch-length. A Brownian fluctuation can then cause the molecule to flip leading to a negative orientation angle θ (see Fig. 4) and the molecule starts recoiling. After the polymer tumbles, the cycle begins anew. The frequency of this cyclic motion was found to be proportional to $Wi^{0.66}$.
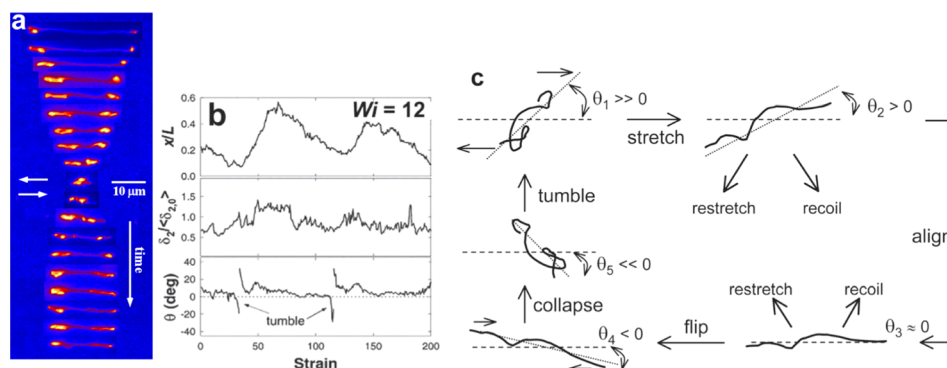

FIG. 4. (a) DNA molecules under shear flow ($Wi = 109$) showing the end-to-end tumbling motion. Time between images is ~ 10 s. (b) Fractional polymer extension x/L, gradient-direction polymer thickness δ_2, and polymer orientation angle θ. (c) Schematic cycle of periodic polymer motion. Reproduced with permission from Schroeder et al., Phys. Rev. Lett. **95**, 18301 (2005). Copyright 2005 American Physical Society.[78]

In contrast to steady shear flow, it is well known that in startup shear flow semi-dilute and concentrated polymeric fluids display a transient stress overshoot at $Wi > 1.0$. Hur *et al.*[79] combined single-DNA measurements with a bulk rheological test and Brownian dynamics simulations to study the dynamics of both dilute and semi-dilute polymer solutions in startup shear flow. They observed an overshoot in the ensemble-averaged molecular extensions at high flow rates (above a critical $Wi \sim 20$) following an overshoot in shear viscosity for semi-dilute polymer solutions ($C \sim 0.5$, 1.0, and 6.0 C^*).

b. Shear thinning and wall slip in concentrated solutions. Understanding the flow behavior of entangled linear-chain polymers has become a main goal in the development of a constitutive model in the polymer rheology. Teixeira *et al.*[66] applied steady shear, and startup shear flow to entangled DNA solutions ($C \sim 31 C^*$) consisting of both fluorescent DNA chains as well as unstained background chains. This allowed them to perturb both the fluorescent test chains as well as the background chains. They employed the single-molecule approach to identify the molecular conformations at different shear rates. They found that DNA molecules displayed highly individualistic behavior with a broad conformation distribution at high Wi in the shear thinning regime ($Wi > 1.0$).[66] Recently, Boukany *et al.*[80] employed a confocal-rheoscope to directly image the DNA conformations in well-entangled DNA solutions ($C \sim 80$ and 160 C^*) during startup shear flow in the stress-overshoot regime ($Wi > 1.0$). They found that adsorbed DNA chains stretched at the surface and disentangled from other chains which remained coiled in the bulk even at $Wi \sim 7$. This interfacial disentanglement led to strong wall slip and transient stress overshoot across the gap ($\sim 50 \mu$m) at $Wi > 1.0$.

3. Dynamics of DNA in contraction flow

Polymeric flows through a contraction are highly relevant in numerous applications, such as polymer processing, extrusion, or injection molding, to name a few. In biological lab-on-a-chip applications such as DNA sequencing, one or many microfluidic contractions can exist. Therefore, understanding the molecular picture leading to macroscopic flow features, such as vortex formation and instabilities, is crucial for optimal performance of the lab-on-a-chip device.

Hemminger *et al.*[47] used calf thymus (75 kbp) DNA solutions to extensively probe flows through a 4:1 planar microfluidic contraction over a wide range of entanglements per chain, $Z = 7$–55 (or $16 C^* < C < 160 C^*$), and over a wide range of Wi ($0.7 < Wi < 21200$). Fig. 5 shows the flow regimes on a Wi–Re space, which were observed for different concentrations of the DNA. For weakly entangled solutions, the critical Wi for vortex formation was found to be $Wi_{cr} \sim 3$. They reported that most of DNA chains remained coiled in the vortex flow. A new flow regime was observed for well-entangled solutions that shows solid-like breakup (coined as jerky-shear banding). In this regime, considerable stretching of the DNA occurred in the strong local flow at the center-line of the contraction channel. However, the DNA in the weak local flow at the corner of the contraction channel underwent quasi-periodic transition from partially coiled to fully stretched. These observations suggested that the DNA chains at the corner disentangle from chains in the center-line. Examining the new jerky-shear banding flow regime using DNA tracers enabled ruling out many microscopic hypotheses that cause flow instabilities such as flow-induced demixing, chain migrations, and chain scission.[47]

More recently, Gulati *et al.*[81] studied flows in semi-dilute and entangled ($C \sim 10 C^*$) DNA solutions in microfluidic gradual contraction over $0.1 < Wi < 446$. No vortex was observed for non-shear thinning DNA solutions over the entire range of Wi numbers. In the case of entangled DNA solutions, the critical Wi for vortex formation in gradual contraction was reported to be $Wi_{cr} = 8.9$. In general, the Wi_{cr} for vortex formation in contraction geometry is in the order of 1–10 at any polymer concentration.

Interested reader can find further information in comprehensive reviews covering both experimental and numerical efforts aimed to explore the flow through contraction.[82–84]
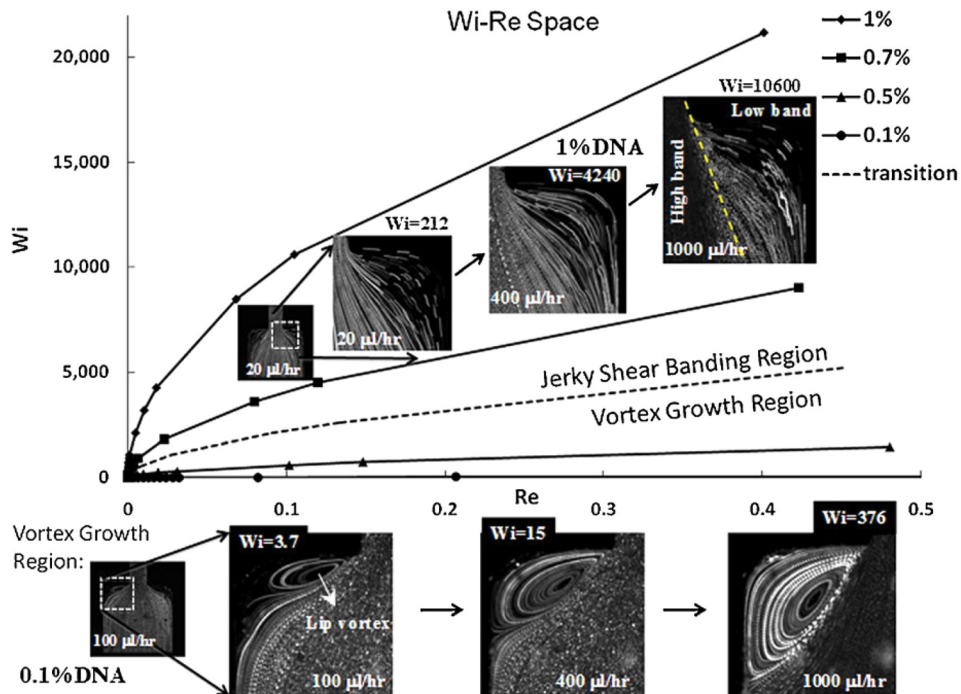
FIG. 5. Summary of the flow behavior in overall *Wi–Re* space for four different solution concentrations of calf thymus DNA (75 kbp). Reproduced with permission from Hemminger *et al.*, J. Non-Newton. Fluid Mech. **165**, 1613 (2010). Copyright 2010 Elsevier.[47]

4. Coil–stretch transition at high Wi in random flow and flow around obstacles

Polymeric flows above *Wi* of O(1), typically exhibit a number of intriguing flow phenomena such as vortex formation and wobble, die swelling, and drag reduction in industrially relevant flows. Molecular visualization of polymer conformations in a random flow relevant to industrial applications will provide valuable information that can be used for optimization of polymer processing. Subsection II D 3 considers flow instabilities in contraction geometry that occur at the critical *Wi* number of around 10. In this case, the perturbation of polymeric flow due to the contraction leads to the transition from a creeping flow field to an unstable flow field consisting of vortices. Groisman and Steinberg[85] showed that strong instability could occur even in the case of homogenous flows of a dilute solution of high molecular weight polyacrylamide (PAA 18 MDa, 80 ppm) between two parallel plates. This instability has all the features of developed classical turbulence, such as hysteresis, power-law scaling of the spectral density curves, albeit at low *Re*. Owing to this resemblance, this flow instability was termed as elastic turbulence. Following the seminal work of Groisman and Steinberg, the elastic turbulence has been observed in polymeric flows for *Wi* > 10 in many other geometries.

Polymer stretching in elastic turbulent flows could be quantified and visualized by using DNA as a molecular probe. It was found that DNA molecules are stretched sharply in a 3D random flow at high *Wi*, via the coil–stretch transition.[86,87] At high *Wi*, the probability distribution function of the normalized polymer length was found to be highly skewed towards 1, i.e., most of the polymer molecules were fully stretched, with the maximum probability occurring at a stretch length of 0.85.[86,88] In contrast to this, in shear flow, the probability distribution function of the polymer length was found to be symmetric at similar value of *Wi*.[86]

Recent experiments on polymer flows through straight microfluidic channels also showed transition to elastic turbulence,[89] provided that the flow was initially perturbed.[90] These experimental observations on instabilities in flows without curvature are supported by nonlinear stability analysis.[91–93] By using DNA as probes, it was found that the polymer exhibits a variety of conformations during flow. In particular, stretching of up to 0.5 (normalized by contour length)
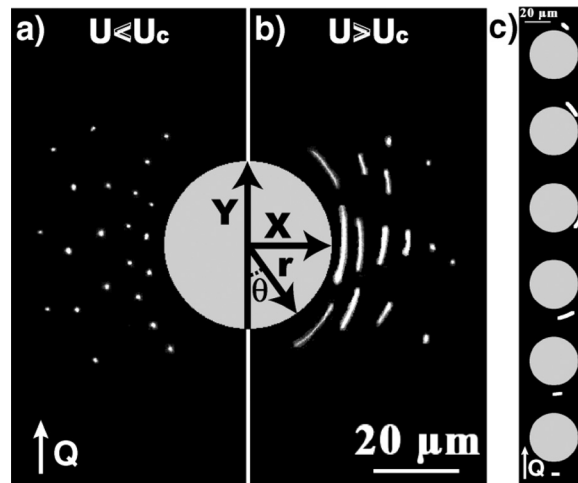
FIG. 6. Polymer conformations near a cylinder (a) below and (b) above the critical $Wi \sim 0.3$ showing significant extensions and transition to coil–stretch. (c) DNA conformation at various locations around the cylinder. Reproduced with permission from François *et al.*, Phys. Rev. Lett. **100**, 18302 (2008). Copyright 2008 American Physical Society.[48]

length units in both parallel and perpendicular direction to the flow has been reported.[214] Since polymer conformation has been linked to elastic stresses in the fluid,[94,95] which in turn provides the driving force for elastic turbulence,[85] the mechanism could be validated by visualizing polymer conformation in straight channels.

The significant reduction of drag by the addition of very small amounts of polymers in a turbulent fluid stimulated both engineers and rheologists, because it lies at the intersection of turbulence and rheology field. This well-known phenomenon has found various applications in the reduction of energy loss in pipelines, ship-building industry, and oil-well fracturing processing.[96] Different mechanisms such as the modification of boundary layer flow or the ability of polymers to stretch (in strong flow) have been proposed to explain this phenomenon.[97–99]

Curved boundaries can also affect the flow response of polymer solutions. For instance, it has been shown that drag on an obstacle (sphere or cylinder) can be significantly enhanced by addition of polymers. The key step to unravel the mechanism behind this phenomenon was to employ single-molecule experiments combined with microfluidic technology. François *et al.*[48] visualized DNA conformations in a microfluidic geometry with a cylindrical obstacle, which revealed strong polymer extensions near the cylinder surface (Fig. 6) coupled with velocity fluctuations indicating transition to an elastic instability.

Using similar microfluidic configuration, François *et al.*[100] subsequently studied polymer conformation and hysteresis in pressure-driven flow of polymer solutions. The motivation to use a cylinder was to study the effect of nonlinear drag forces. Combining an optical fiber sensor, which allowed measurements of the stresses on the cylinder due to polymer flow, together with fluorescence microscopy, they were able to link the molecular picture of polymers to the macroscopic effect of hysteresis upon stopping the flow. They reported that when the flow was stopped, the polymer molecules near the cylinder reversed their flow due to stored elastic stresses in the molecule. Several other studies on flow around obstacles and their arrays are reported for electrokinetic flows. These studies have been reviewed in detail elsewhere.[16]

E. Stretching of DNA molecules on micropatterned surfaces

Not only that stretching of DNA is highly relevant for polymer rheology and genomic analysis, it also can be used to generate nanowire or nanotemplate arrays. DNA chains can be fully stretched across micropillars in de-wetting flow over micropatterned surfaces.[101] This is a simple and yet powerful technique (referred to as molecular combing) for stretching DNA molecules on solid substrates by forced de-wetting. This technique was originally used to visualize DNA in an elongated conformation after depositing DNA molecules on solid substrates.[102] In
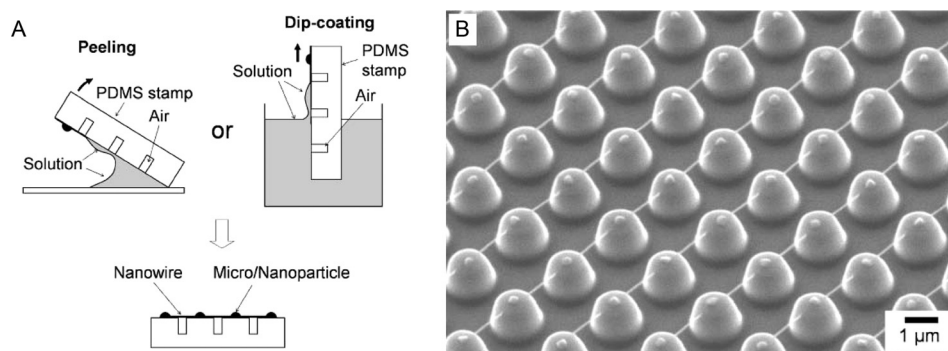
FIG. 7. (a) Schematic illustration of DNA combing for generating a nanowire array. (b) Scanning electron microscope (SEM) images of an array of DNA nanowires. Reproduced with permission from Guan *et al.*, Soft Matter **3**, 1369 (2007). Copyright 2007 The Royal Society of Chemistry.[103]

comparison to traditional combing technique, long macromolecules in a solution can be immobilized into ordered array of nanowires by de-wetting of micropatterned surfaces (Fig. 7).[103–106] Stretching of DNA is a prerequisite process to create and deposit elongated DNA molecules on top of a micropatterned substrate. The formation of a droplet on the top of microstructured surfaces such as micropillars during the de-wetting process produces a flow pattern allowing stretching DNA across the micropillars.[101] In addition, Guan *et al.*[107] demonstrated that DNA nanowires can be converted into nanochannels by the imprinting method. To summarize, this simple technique has a great potential for low-cost fabrication of nanofluidic systems without size limitations.

III. DNA IN NANOFLUIDIC SYSTEMS

The transport of biomolecules through nanoscale structures is crucial in many biological processes. Illustrative examples range from the passage of DNA and RNA through the nuclear-pore complexes, ejection of DNA from a virus head into a host cell, to transport of proteins across the plasma membrane.[108,109] Natural or synthetic nanoscale structures can confine DNA in spaces far below its typical bulk equilibrium size, influencing its equilibrium and dynamic properties. For instance, the DNA becomes stretched at equilibrium when confined inside a nanochannel, which makes nanochannels an ideal geometry for high-throughput DNA linearization, and particularly suited for optical DNA mapping.[24] Research on DNA confinement in nanofluidic systems has therefore been largely driven by the interest in studying various phenomena in cell biology[110] as well as for developing different biomedical applications based on single-molecule analysis. In addition, great interest comes from the perspective of polymer physics, for which the DNA is highly useful as a model system.

In a typical experiment, a dilute concentration ($\sim$picomolar) of DNA molecules is introduced into a microfluidic reservoir via a pipette and driven into or through a nanostructure by means of a pressure gradient or an electric field. Amongst various forms of nanostructures developed to manipulate the behavior of DNA,[23,111–114] we specifically focus on nanoslits, nanochannels, and nanopores (Fig. 8). We first introduce the fundamental physics, which governs the conformation of the DNA confined inside a nanoslit or a nanochannel (Section III A 1). Understanding how the DNA conformation depends on the characteristic dimensions of the nanoslit/channel is an important precondition for designing efficient nanofluidic concepts for DNA manipulation. Few examples of nanofluidic concepts used for stretching the DNA and for separating DNA molecules with different molecular length are then given in Section III A 2. Next, we address the transport of DNA through nanopores, which has been extensively explored for the purpose of DNA sequencing (Section III B). Finally, we touch upon the use of nanofluidics for DNA transfer into live cells, which involves a complex sequence of driving the DNA through a nanochannel and across the cell membrane into the cell interior (Section III C).
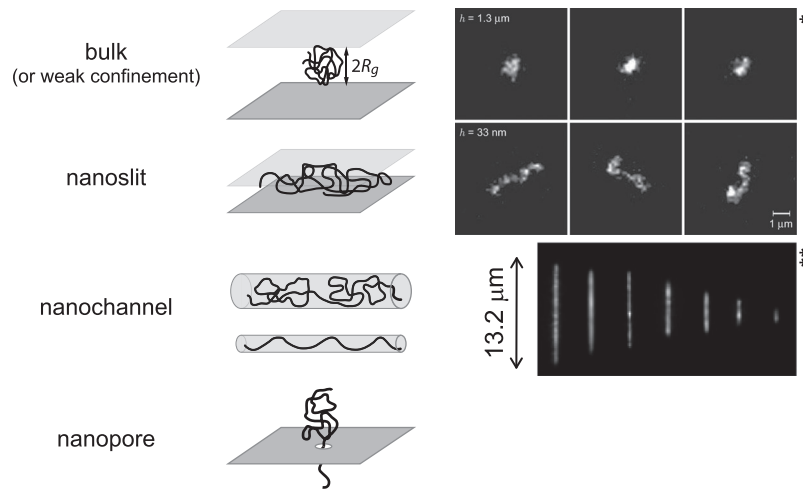
FIG. 8. Schematic representation of different nanostructures used for confining the DNA (left) and the corresponding fluorescence images of the DNA under confinement (right). A nanoslit is characterized by one nanoscale dimension (height), a nanochannel by two nanoscale dimensions (height and width), and a nanopore by three nanoscale dimensions with axial symmetry (radius and length). (*) λ-DNA in 1.3 μm high (first row) and 33 nm high (second row) nanoslits. Reproduced with permission from Bonthuis *et al*., Phys. Rev. Lett. **101**, 108303 (2008). Copyright 2008 American Physical Society.[115] (**) λ-DNA in nanochannels with different cross-section. From left to right the cross-section increases from 30 nm × 40 nm to 440 nm × 440 nm. Reproduced with permission from Reisner *et al*., Phys. Rev. Lett. **94**, 196101 (2005). Copyright 2005 American Physical Society.[116] Schematic representation was inspired by Hsieh and Doyle.[117]

A. Nanoslits and nanochannels

1. Physics of confined DNA: From the Odijk to the de Gennes regime

After intense experimental and theoretical efforts, the fundamental physics of DNA confined in nanoslits and nanochannels became rather well understood (for a recent comprehensive review, see Dai *et al*.[118]). Confining the DNA within a structure with length scale D (either nanochannel diameter or nanoslit height) smaller than the unperturbed coil size of DNA causes the DNA to deform and stretch. First, let us consider how free DNA behaves in solution. According to the Flory theory, the equilibrium size of an unperturbed DNA molecule (radius of gyration, R_g) in solution can be estimated from the balance of entropic effects and excluded volume effects of the DNA segments. Entropic effects act to minimize the volume of the DNA coil. The excluded volume effects arise from the fact that the segments have a finite size and cannot overlap with each other, which causes the chain to swell. Based on this argument, R_g of the free DNA in a good solvent is given as: $R_g \sim (w_{eff}\, 2P)^{1/5} L^{3/5}$, where w_{eff} is the effective width, P is the persistence length, and L is the contour length of the chain.[119,120] When confined, the equilibrium properties of the DNA follow various scaling regimes (Fig. 9(a)), which are made by the competition of the bending energy (elastic entropy), excluded volume interaction, and confinement.

The basic principle of DNA confined inside a channel with dimensions smaller than the radius of gyration ($D < R_g$) is traditionally described in terms of blob-partitioning in large channels (de Gennes regime) and chain deflection in very narrow channels (Odijk regime).[121,122] In the de Gennes regime ($P < D < R_g$), the conformation of the chain can be understood as a series of non-interacting spherical blobs with size D.[62] These blobs avoid each other due to excluded volume effects. The sub-chain inside each blob, however, behaves as it would in free solution. Therefore, the sub-chain follows the Flory scaling, $L_{blob} \sim D^{5/3}$, where L_{blob} is the contour length inside a blob. This argument predicts the extension $\langle x \rangle$ of a moderately confined DNA that scales with D as $\langle x \rangle \sim L(w_{eff}\, P/D^2)^{1/3}$. On the other hand, in the Odijk regime, where the channel dimension is smaller than the DNA's persistence length ($D < P < R_g$), the DNA deflects back and forth from the channel walls. Therefore, the physics is dominated by the interplay between confinement and entropic forces (DNA elasticity), and not by excluded volume effects.[121]
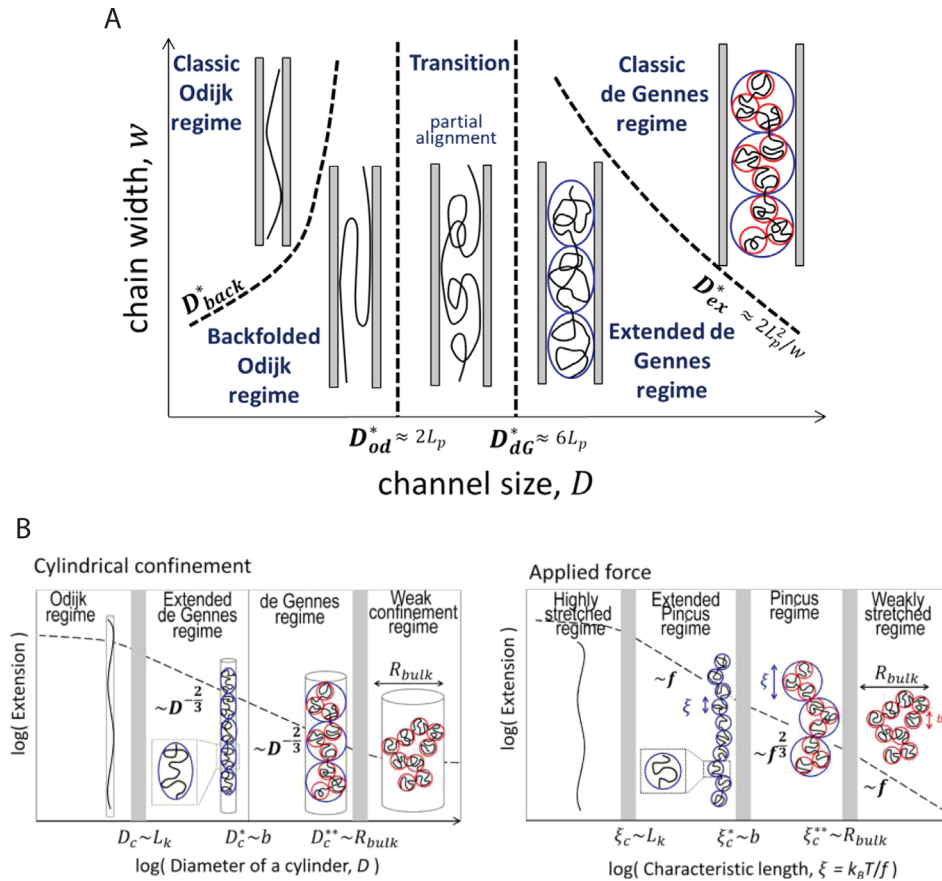
FIG. 9. (a) Schematic illustration showing different regimes of confined DNA in a tubular channel when varying the channel diameter and the chain width. The black curves represent polymer chains, red circles represent thermal blobs, and blue circles or ellipses represent the self-avoiding blobs. The dashed lines represent the boundaries between the regimes. Reproduced with permission from Dai *et al.*, Adv. Colloid Interface Sci. **232**, 80 (2016). Copyright 2016 Elsevier.[118] (b) Similarities between extension of a polymer in a channel (left) and tensile constraints on a polymer (right). Reproduced with permission from L. Dai and P. S. Doyle, Macromolecules **46**, 6336 (2013). Copyright 2013 American Chemical Society.[127]

In this regime, the extension of the DNA can be predicted as $\langle x \rangle \sim L(1 - A(D/P)^{2/3})$, where the pre-factor $A \sim 0.17$–0.18 is a constant that has been determined numerically by simulations for channels with either square or circular cross-section.[123] In addition, the DNA enters the back-folded Odijk regime, if the bending energy and excluded volume effects are not sufficiently strong to prevent back-folding. Experimental studies of confined DNA are usually located in the intermediate region between the Odijk and the de Gennes regime.

Recently, Wang *et al.*[124] used Monte Carlo simulations to simulate the extension of DNA in nanochannels and suggested the "extended de Gennes regime" in the transition region (Fig. 9(a)). In this regime, the DNA can be considered as a string of elongated anisometric blobs. The DNA chain enters the extended de Gennes regime as the repulsion between the blobs weakens compared to the classic de Gennes regime. The crossover from the classic to the extended de Gennes regime can be identified by equating the excluded volume interaction between two blobs with the thermal energy, k_BT.[124,125] Simulations have validated the prediction of extension, fluctuations and confinement free energy in the extended regime.[126–128]

From the viewpoint of the scaling analysis, polymers in cylindrical confinement share some similarities with polymers under tension[127] (Fig. 9(b)). The scaling regimes for polymers under tension can be categorized in the classic Pincus, extended Pincus, and highly stretched regime, which are analogous to the classic de Gennes, extended de Gennes, and Odijk regime for polymers in confinement. In the classic Pincus regime, the tensile force f applied to the end of

a polymer introduces a characteristic length $\xi = k_B T/f$, which is very similar to the effect of the channel diameter in the classic de Gennes regime. In the classic Pincus regime, extension scales with force as $\langle x \rangle \sim f^{-2/3}$ which is comparable to $\langle x \rangle \sim D^{-2/3}$ in the classic de Gennes regime. However, the scaling of extension $\langle x \rangle \sim f$ in the extended Pincus regimes is different from the scaling in the extended de Gennes regime ($\langle x \rangle \sim D^{-2/3}$).[127] This difference in scaling originates from different forces driving to separate the blobs. If the DNA is confined, the blobs are segregated by excluded volume interaction. In this case, if the blobs are smaller than the thermal blob size b (size where the excluded volume interaction equals $k_B T$; indicated by red circle in Fig. 9), repulsion between two blobs is not sufficient to segregate them. If the DNA is under tension, the blobs are separated by the imposed tensile forces. In this case, even if the blob is smaller than the thermal blob, the underlying physics is still dominated by the tensile forces.[119,127]

The extension of the DNA in confinement is not only influenced by the characteristic dimensions of the confining geometry, but also by the ionic strength of the aqueous buffer. The Debye length of the electric double layer increases with decreasing salt concentration, meaning that the charges are screened over longer distances. As a result, the persistence length and the effective width of the DNA increases and the excluded volume effects are higher.[129,130] Buffers with lower ionic strengths thereby lead to enhanced stretching of the DNA.[24,131]

The conformation of confined DNA is moreover affected by the presence of crowding agents such as dextran.[132,133] When increasing the concentration of the crowders, the DNA molecule progressively stretches, because the crowders occupy the free volume along the nanoslit/channel walls, effectively reducing the nanoslit/channel dimensions. However, when the concentration of the crowders exceeds a certain value, the behavior of the DNA changes. In nanoslits, the DNA starts to compress with further increase in the concentration.[133] In nanochannels, the DNA abruptly condenses into a compact form above a certain threshold concentration.[132,133]

2. Manipulation of the DNA inside nanoslits and nanochannels under an applied force

As explained in the Section III A 1, confinement of the DNA inside nanoslits and nanochannels results in stretching of the DNA at equilibrium. In this section, we will further provide few examples of how the DNA can be manipulated by inducing an external flow through the nanoslit/channel by means of an applied pressure or an electric field. The aim is not to provide an extensive review but to demonstrate few recently developed concepts of DNA manipulation, which can be used for various biomedical/technological applications. Thorough reviews on the applications of nanoslits and nanochannels for DNA manipulation can be found elsewhere.[23,24,134,135]

We have already mentioned above that DNA linearization by equilibrium stretching inside a nanochannel is particularly suited for optical mapping of the genetic information along the DNA molecule.[24,27–29,134,136] An optical map is obtained by fluorescently labeling specific parts (sequence motifs) along the DNA and can be used to identify structural variation in a genome, compare genomes, or detect pathogens. Stretching the DNA at equilibrium, however, has certain limitations. The DNA does not stretch to its full contour length and the captured fluorescence signal is noisy due to the Brownian motion of the DNA.[28] Marie *et al.*[137,138] proposed a lab-on-a-chip design that overcomes these limitations. Their device operates in three successive phases (Fig. 10). In the first "selection" phase, the DNA molecules are transported through a microchannel by pressure-driven flow. In the second "isolation" phase, the selected DNA strand is forced inside a $440\,\mu$m long, $85\,$nm shallow nanoslit by increasing the pressure inside the microchannel. In the final "stretching" phase, the inserted DNA molecule is elongated via a perpendicular elongational flow from the side-arms of the cross-shaped nanoslit. The hydrodynamic drag applies a force on the DNA in the pN range, which is sufficient to stretch the DNA up to 98% of its full contour length, which is more that can be achieved by equilibrium confinement.[139] In addition, the high tension of the DNA as well as the confinement within the nanoslit represses the DNA's Brownian motion, enabling superior spatial resolution during fluorescence
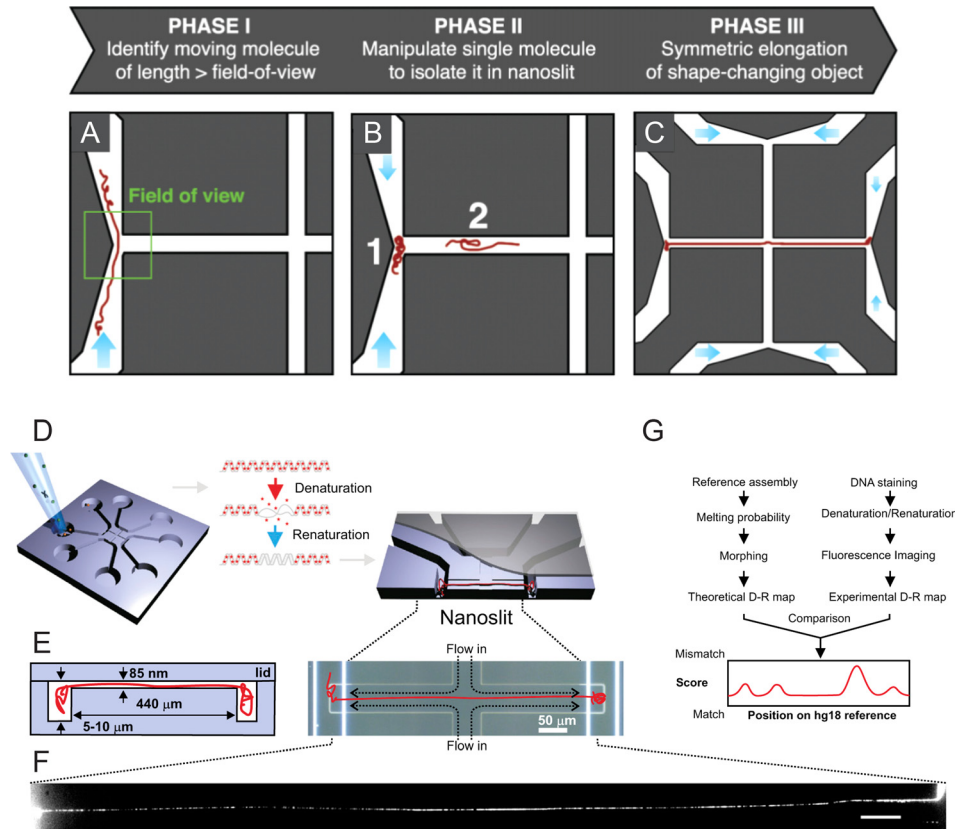
FIG. 10. Fluidic chip design for DNA linearization and optical mapping. (a)–(c) Schematic representation of the main concept: (a) the DNA is pressure-driven through a microchannel to the nanoslit entrance, (b) loaded into the nanoslit by increasing the pressure inside the microchannel, and (c) elongated via pressure-driven flow from a second, perpendicular nanoslit. Fluorescence images from each phase can be used to automate the DNA manipulation procedure by real-time image processing. Reproduced with permission from Sørensen *et al.*, Rev. Sci. Instrum. **86**, 63702 (2015). Copyright 2015 AIP Publishing LLC.[138] (d)–(f) The nanofluidic concept can be used for optical DNA mapping, as shown by the following example. (d) The chip is loaded with cell extract enriched in chromosomal DNA. Stained DNA is partially denatured and renatured in order to create a fluorescence pattern (see (f)). (e) The inlet ports of the chip connect to 5- to 10-μm-deep microchannels for DNA handling, which feed into an 85-nm shallow nanoslit. After stretching the DNA inside the nanoslit, the DNA is imaged. (f) The fluorescence image of a megabase pair-long DNA fragment shows a "barcode" where bright areas correspond to regions rich in cytosine-guanine, whereas dark areas correspond to regions rich in adenine-thymine. (g) The fluorescence pattern is compared to the pattern from the reference genome. Reproduced with permission from Marie *et al.*, Proc. Natl. Acad. Sci., U.S.A. **110**, 4893 (2013). Copyright 2013 National Academy of Sciences, USA.[137]

imaging. They further showed that the entire process of DNA manipulation could be automated based on real-time processing of fluorescence images.[138]

Nanochannels and nanoslits can also be used to separate DNA molecules with different molecular lengths.[140,141] One option is to flow the DNA molecules through a nanochannel by means of a pressure gradient. The separation is possible since, within a nanochannel with given dimensions, shorter DNA molecules have a lower hydrodynamic mobility compared to longer DNA molecules. More specifically, Wang *et al.*[141] identified four distinct regions of DNA mobility, when driving DNA (10 bp to 1.9 Mbp) through fused-silica capillaries (long nanochannels) with radius of 750 nm; these regions were named rod-like, free-coiled, transition, and constant mobility region (Fig. 11(b)). The rod-like region corresponds to DNA shorter than its persistence length (∼150 bp). The free-coiled region corresponds to DNA, for which the effective hydrodynamic radius scales with molecular length as characteristic for freely coiled polymers (∼150–2000 bp). In these two regions, the DNA mobility monotonically increases with the size of the DNA, which can be intuitively explained considering the fluid velocity profile, generated by the applied pressure gradient (Fig. 11(a)). When two particles with different size are carried by Poiseuille flow inside a confined geometry, the larger particle on average moves faster
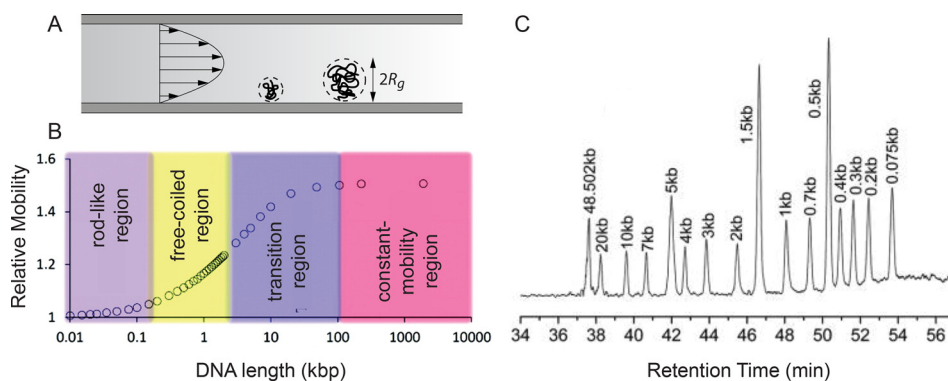
FIG. 11. (a) Schematic illustration of the mechanism by which larger DNA coils move faster through the capillary when driven by pressure. (b) General relationship between DNA relative mobility and its molecular length within a capillary with radius of 750 nm. (c) Chromatogram corresponding to separation of a mixture of DNA with different molecular lengths. The separation capillary had a radius of 750 nm and a total length of 50 cm. Adapted with permission from Wang *et al.*, J. Am. Chem. Soc. **134**, 7400 (2012). Copyright 2012 American Chemical Society.[141]

because its center of mass cannot approach the wall (where the flow is the slowest) as close as the smaller particle. Hence, DNA molecules with larger effective size require a shorter amount of time to exit the capillary, which enables separation of DNA molecules based on their molecular length (Fig. 11(c)). However, DNA molecules, which have a bulk hydrodynamic radius larger than the capillary radius (>100 kbp), cannot be separated. These molecules belong to the constant mobility region. The molecules in the constant-mobility region are forced to deform into a "cylinder" inside the narrow capillary; they are stretched along the axis and stay preferentially in the middle of the capillary. In order to separate longer DNA molecules, one would simply need to use a wider capillary.[142,143] Wider capillaries, however, exhibit reduced resolution for short DNA fragments. Therefore, combined use of narrow and relatively wider capillaries could provide a solution for separation of DNA molecules over a wide range of molecular lengths, which provides an attractive alternative to gel electrophoresis.[144] Major advantages of DNA separation using such capillaries as compared to gel electrophoresis are low sample and reagent consumption, simple and inexpensive apparatus, high efficiency and resolution, elimination of sieving matrices, and long column lifetime.[143]

Another interesting approach of DNA separation, yet very different from the one described in the preceding paragraph, was shown by Gupta *et al.*[145] The approach involves driving the DNA molecules electrophoretically through nanochannels (200 nm × 400 nm × 10 μm) shorter than the length of the stretched DNA. The separation mechanism relies on the fact that the DNA must uncoil in order to enter a nanochannel smaller than its radius of gyration.[146,147] Consequently, longer DNA molecules require more time to translocate the nanochannel than shorter molecules. Gupta *et al.*[145] demonstrated the main concept based on the following example. When they applied a single monopolar pulse (4 V, 200 ms), shorter λ-DNA (48.5 kbp) could completely migrate through the nanochannel, whereas longer T4-DNA (166 kbp) could not transverse the entire nanochannel and remained "trapped" with the ends of the chain hanging from the nanochannel inlet and outlet (Fig. 12). The trapped T4-DNA was in quasi-equilibrium after the end of the pulse since both ends of the DNA were pulled by equal and opposite entropic recoiling forces exerted by the portions of the DNA outside the nanochannel. Eventually, the forces on one side of the nanochannel prevailed and the DNA retracted and recoiled on one or the other side of the nanochannel within 16–18 s. To speed up the T4-DNA recoiling process and to control its direction back towards the nanochannel inlet, they used an asymmetric bipolar pulse. The forward bias of the pulse was the same as before (200 ms, 4 V) allowing λ-DNA to fully translocate and T4-DNA to only partially translocate the nanochannel. The parameters of the reverse bias (0.1 V, 10 s) were tailored such that the electric field inside the nanochannel was sufficiently high and the pulse sufficiently long to pull T4-DNA back to the inlet side. At the same time, the amplitude of the reverse bias was small enough to prevent
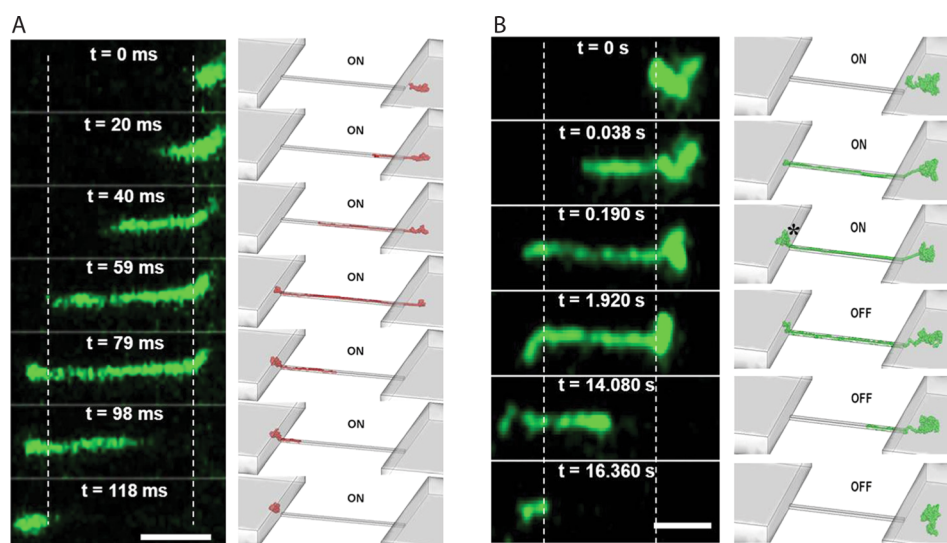
FIG. 12. DNA dynamics under a single forward pulse of 4 V and 200 ms. Snapshots of λ-DNA (a) and T4-DNA (b) from experiments and from corresponding Brownian dynamics simulations (right). Dashed lines in fluorescence images mark the nanochannel inlet and outlet. Scale bar 5 μm. Reproduced with permission from Gupta *et al.*, Biomicrofluidics **8**, 24114 (2014). Copyright 2014 AIP Publishing LLC.[145]

λ-DNA from re-entering the nanochannel. Namely, the DNA has to overcome an entropic barrier when entering the nanochannel; in the given system, a threshold voltage of 0.4 V was required for surpassing this entropic barrier.

Further possibilities for DNA manipulation can be achieved by introducing complex geometries into nanoslits, such as nanocavities, which act as entropic traps for the DNA. Such traps can be used, e.g., for immobilization and control of local DNA conformation, or for DNA separation. We will not go into further details, but we refer the reader to recent work related to this topic.[23,148,149]

B. Nanopores

Nanopores are highly interesting as sensors of different molecules such as nucleic acids, proteins, and drugs.[150–154] Translocating a molecule through a confined nanopore provides an effective tool to *read-off* sub-molecular information based on various noncovalent bonding interactions of the molecule with the pore wall, including hydrophobic interactions, aromatic interactions, electrostatic interactions, and hydrogen bonding.[154] The most widely exploited sensing approach mimics the concept of the Coulter Counter,[155] originally used for counting and sizing micrometer-large particles suspended in an electrically conducting fluid by passing them one-by-one through a constriction. The general idea is depicted in Fig. 13. A thin perforated membrane is placed between two salt solutions and a high-bandwidth voltage-clamp amplifier is used to generate a voltage across the membrane and measure the ionic current through the nanopore[156] (Fig. 13(a)). In addition, the transmembrane voltage provides an electrophoretic force to drive charged molecules, such as DNA, through the pore. As the molecule enters the pore, it partly blocks the path for small ions, consequently reducing the measured electric current (i.e., it induces a transient "current blockade," Fig. 13(b)). Statistical analysis of the magnitude and duration of these transient current blockades provides information on the physicochemical properties of the translocating molecules, such as their length and the strength of their interactions with the pore surface.[154,157] Although the electric current in most of the cases decreases once the molecule occupies the pore, it has also been observed that under certain conditions (specifically at low ionic concentration, roughly below 0.4 M) the electric current increases or exhibits a biphasic signal during DNA translocation.[158–160] The increase in electric current is at least partially mediated by increased concentration of positive counterions, which
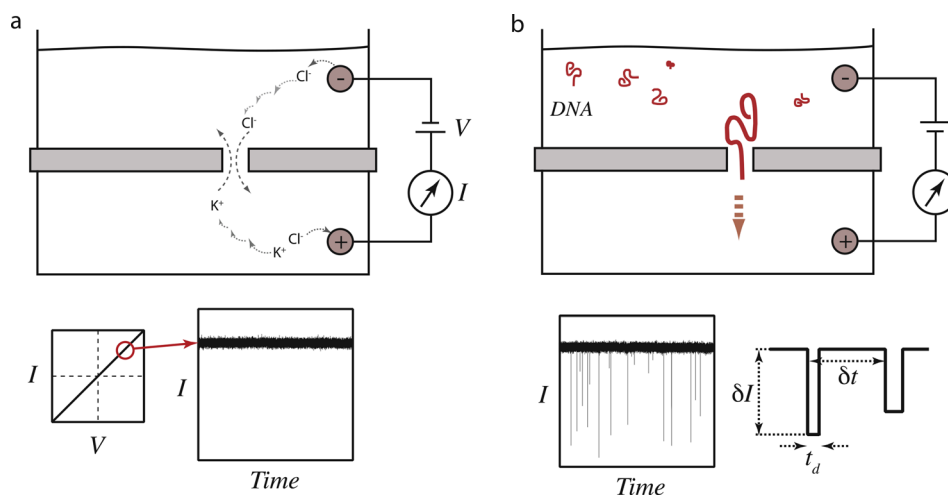
FIG. 13. Basic concept of sensing molecules with nanopores. (a) Application of a voltage across the membrane induces a steady electric current carried by small ions passing through the pore. (b) When charged molecules, such as DNA, are added to the chamber, the transmembrane voltage electrophoretically attracts the molecules into the pore. The molecules stochastically enter the pore, producing a measurable "electric current blockade." First-order parameters that can help in characterizing the sample are the dwell time (t_d), the average current blockade amplitude (δI), and the time between successive blockade events (δt). Reproduced with permission from M. Wanunu, Phys. Life Rev. **9**, 125 (2012). Copyright 2012 Elsevier.[164]

are attracted by the negatively charged DNA into the pore.[161,162] Nevertheless, the microscopic origins of this non-intuitive phenomenon are not yet completely understood.

The characteristic signal of the current blockade indeed depends on numerous variables: the pore size, geometry, ionic conditions on each sides of the membrane, chemical associations and charge condensations on the pore, ionic condensation on the molecule, magnitude of the transmembrane voltage, and temperature.[163] Some of these variables can change during the course of the experiment, which makes it challenging to theoretically describe and analyze the full details of the current blockade phenomenon by currently available theoretical and computational tools.[163]

For the DNA (or any other polymer), the translocation through the pore is an activated process with an entropic barrier;[165–167] the DNA, namely, enjoys many more configurational possibilities in the bulk than within the pore. The translocation dynamics can be divided into three distinct stages: (i) approach of the DNA to the pore opening, followed by repeated threading and unthreading of one of its ends into the pore, (ii) a final threading ('capture') into the pore, and (iii) the eventual translocation event.[163] In the electric current signal analysis, the repeated threading–unthreading events are filtered out and only the change in the current after the capture of DNA into the pore is taken into account. The translocation event, which determines the signature electric current blockade, is controlled by external fields/forces, DNA dynamics, and DNA–pore interactions.[163]

Since the blockade signal depends on the DNA properties, it can be used to evaluate the purity and phosphorylation state of nucleic acid preparations,[168] for analysing unzipping kinetics of double-stranded DNA and hairpins,[169–171] DNA polymerase activity,[30,172] or DNA–protein interactions.[173] The most prominent application of threading the DNA through a nanopore, is though DNA sequencing.[164,174–176] The idea, initially proposed in the 1990s,[177] relies on the discrimination of nucleotides based on their different current signatures, when single-stranded or double-stranded DNA is transferred through the pore in a linear fashion. The nanopore approach, which does not require any labels or amplification, is nowadays developed to the extent to be considered as an option for the fourth-generation low-cost and rapid DNA sequencing technology, with the potential of quickly and reliably sequencing the entire human genome for less than $1000 (possibly for even less than $100).[178]

Three main types of nanopores are considered for DNA sequencing: biological protein channels (e.g., α-hemolysin, MspA), solid-state nanopores, and hybrids of the former two[174] (Fig. 14). Nanopores from solid-state materials have obvious advantages over their biological counterparts such as very high stability, control of diameter and pore length, ease of surface
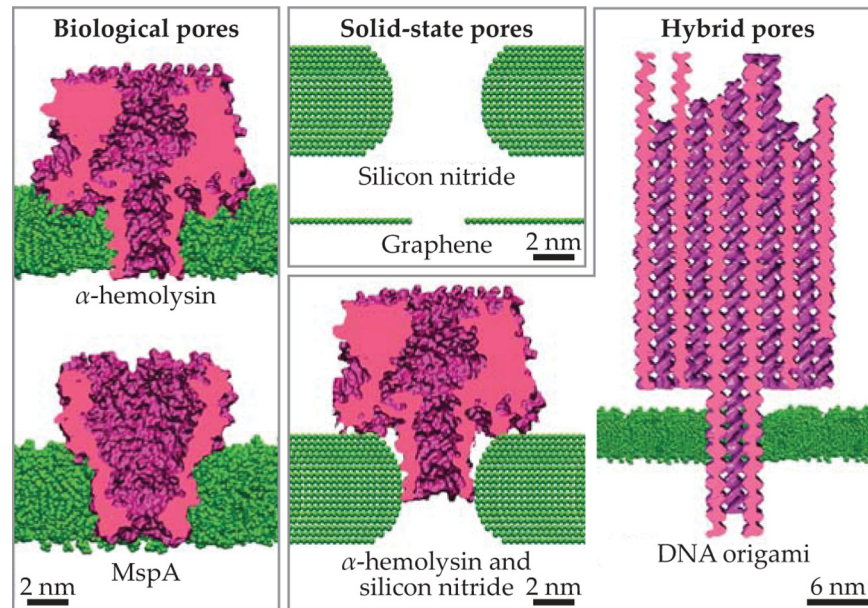
FIG. 14. Three main types of nanopores used for DNA sequencing: biological pores inserted into a lipid bilayer; solid-state nanopores, drilled into thin membranes of silicon nitride, graphene, or other materials; and hybrid pores consisting of biological pores docked into solid-state pores, or DNA-origami pores, which can be docked both into a lipid bilayer or solid-state pore. Silicon nitride membranes are typically thicker than shown in the figure. Images courtesy of Aleksei Aksimentiev and Hendrik Dietz. Reproduced with permission from Muthukumar *et al.*, Phys. Today **68**, 40 (2015). Copyright 2015 AIP Publishing LLC.[175]

functionalization, and the potential for integration into devices and arrays[109] (fabrication techniques of solid-state nanopores were recently reviewed by Kudr *et al.*[179]). Nevertheless, biological pores have a specific, highly selective nonuniform shape, which cannot be fabricated with current technologies. To mitigate this challenge, a viable option is to integrate biological pores into solid-state membranes enabling to combine single-nucleotide recognition capabilities of biological pores with wafer-scale arrays of solid-state nanopores for high-throughput sequencing applications.[174] In the past few years, nanopores synthesized with the DNA origami technique have emerged as another attractive alternative since they offer a highly flexible design of the geometrical and surface properties of the pores.[176,180,181]

Reading the sequence of the DNA is, in fact, non-trivial and cannot be performed by simple threading of the DNA through typical solid-state nanopores. There are two major challenges. The first is the lack of spatial resolution necessary to identify the DNA molecule at the single-base level. The spacing between two neighboring nucleotides is ~ 0.34 nm, whereas the length of typical solid-state nanopores is ~ 20 nm.[182] The measured signal of the current blockade is therefore caused by several bases coexisting in a nanopore. This issue is being addressed by thinning silicon nitride (SiN_x) membranes using electron beam lithography followed by reactive ion etching,[183] or by using atomically thin membranes from graphene,[184] boron nitride[185] (BN), and molybdenum disulfide[186] (MoS_2). Note, however, that even in the MspA pore, which is only ~ 0.6 nm long in its narrowest region, the measured current signal is determined by about four nucleotides at any given time, which requires specific data processing to extract the information from single nucleotides.[187] The second challenge is that the translocation speed of DNA in any type of currently used nanopores is too fast. To compensate for the high frequency noise in the signal, a 10-kHz low-pass filter is usually used to record ionic current, limiting the time resolution of the measurements to $\sim 50\,\mu s$.[182] To achieve sufficient sensitivity for reading distinct nucleotides, the translocation velocity should be in the range 1–100 nucleotides (nt) or base pairs (bp) per ms. Yet, the typical velocity in biological pores and solid-state nanopores with comparable diameter is on the order of 1 nt or bp per μs.[174,188] Other difficulties limiting the sensitivity of the measurements are the random thermal motion of DNA within the pore,[189]

as well as intramolecular velocity fluctuations likely arising from variations in the drag force as the DNA blob outside the pore unfolds.[190]

To reduce the velocity of DNA translocation, several strategies have been proposed (see recent reviews[182,191]). An efficient approach to control the velocity in biological pores is to incorporate an enzyme, which acts as a stepper motor driving the DNA across the pore.[31,192] In this case, the speed of nucleotide reading was reduced to about 40 nt/s or less. As an analogy to enzyme motors in solid-state nanopores, the DNA translocation can be controlled by attaching the ends of the DNA to a polystyrene bead and manipulate its movement by optical[193] or magnetic tweezers,[194] or by attaching the DNA to an AFM tip,[195] which can be controllably inserted into the nanopore. Other approaches, which are more appropriate for parallelized analysis in a nanopore array, include application of a pressure difference in the opposite direction to the electrophoretic DNA motion,[196,197] application of a gate voltage in the nanopore wall to manipulate the electroosmotic flow through the pore,[198] or introduction of agarose gel to the *cis* or *trans* side of the nanopore to retard the DNA movement.[199]

The demands for parallelization of the nanopore readings are indeed high, since a single nanopore working at 10 ms/bp would take about 20 years to sequence a human genome.[200] In order to achieve the required high-throughput parallelized sequencing, Huang *et al.*[201] recently demonstrated that it would be feasible to replace electric current measurements with fluorescence imaging of the ionic current through the nanopores.

C. Using nanofluidics to inject DNA into living cells

Nanofluidic systems can also offer certain advantages for delivery of DNA into cells by means of electroporation.[202,203] Electroporation is a technique, which allows to transiently increase the permeability of the cell membrane by exposing the cell to an electric field. In conventional electroporation protocols, cells in suspension or in tissue are placed between two electrodes to which a voltage pulse (typically hundreds of μs to tens of ms long) is applied. The resulting electric field between the electrodes induces a transmembrane voltage across the cell membrane, which leads to formation of small nanometer-size aqueous pores in the lipid domains of the cell membrane acting as aqueous pathways for exogenous molecules such as drugs or genetic material.[204,205]

The pores in the fluid lipid bilayer are, however, highly dynamic and most of them are expected to collapse within nanoseconds to microseconds after the pulse.[206–208] Consequently, if the DNA is not able to translocate the cell membrane while the pores are still open (i.e., during the pulse), the DNA could get stuck inside the membrane. Indeed, it was experimentally observed that in conventional electroporation approaches, the DNA forms a complex with the cell membrane prior to its translocation.[209] Furthermore, recent studies suggest that, the DNA mainly translocates the membrane by an endocytotic-like mechanism, which takes place during minutes after the electric pulses were applied.[210,211]

Electroporation of cells in a microchannel-nanochannel-microchannel configuration offers a way to bypass the endocytotic pathway in DNA delivery[212] (Fig. 15(a)). It this setup, a cell is placed into one microchannel and positioned next to the nanochannel, e.g., with optical tweezers. The DNA is then placed into the other microchannel. When a voltage pulse is applied across two electrodes immersed into the microchannels, a high electric field is established inside the nanochannel, which provides a strong electrophoretic force to drive the DNA through the nanochannel. Since the fringing field also reaches the cell, it electroporates the cell membrane next to the nanochannel outlet and allows the DNA to be injected into the cell. Although the dynamics of DNA translocation in such setup have not yet been thoroughly investigated, it is speculated that the DNA is able to transverse the nanochannel and translocate through a nanopore in the cell membrane already during the pulse. As the DNA is not endocytosed, the gene expression can be detected within 3 h, which is much faster than in conventional electroporation approaches, where the genes are expressed roughly a day after the cells were exposed to electric pulses. Moreover, the amount of the delivered DNA can be precisely controlled by adjusting the duration and number of applied pulses.
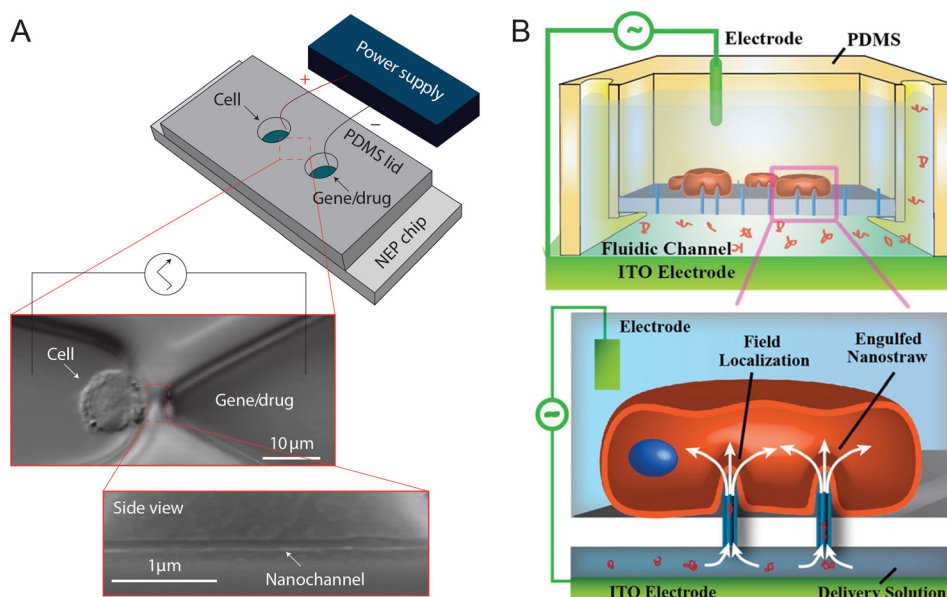
FIG. 15. Nanofluidic electroporation for precise gene delivery into living cells. (a) Nanochannel electroporation setup. Adapted with permission from Boukany *et al.*, Nat. Nanotechnol. **6**, 747 (2011). Copyright 2011 Macmillan Publishers Ltd.[212] (b) Nanostraw electroporation device. Reproduced with permission from Xie *et al.*, ACS Nano **7**, 4351 (2013). Copyright 2013 American Chemical Society.[213]

An alternative approach to nanochannel electroporation is to culture cells on an array of hollow alumina nanostraws connected to an underlying microfluidic channel[213] (Fig. 15(b)). The cells are able to engulf the nanostraws without damaging their membrane. By applying a voltage pulse between the microchannel and the bulk solution above the nanostraw membrane, it is possible to achieve local membrane electroporation at the tip of the nanostraws. This allows the delivery of DNA molecules, which are electrophoretically driven from the microchannel, through the nanostraws, into the cells.

IV. CONCLUSION AND PERSPECTIVE

Micro/nanofluidic systems have been utilized to probe, manipulate, and visualize DNA molecules for various biomedical applications as well as fundamental studies concerning polymer rheology and physics. Recent progress and advances in fabrication of micro/nanofluidics have facilitated the study of polymer rheology at the single-molecule level. We have reviewed a selection of fundamental concepts in the flow of DNA inside microfluidics, which allows us to create a conceptual framework for nonlinear polymer rheology. This field is undergoing unprecedented changes, because DNA with different architecture and topology can be made and can serve as a new model for polymer scientists and engineers. We anticipate that future studies will focus on relating the polymer microstructure to bulk flow properties in flow fields relevant to industry. In addition, new molecular-level experiments would be highly desirable in the flow of well-entangled polymer solution to improve our theoretical understanding in nonlinear flow regimes.[17] Still, nonlinear rheological responses of well-entangled polymer such as shear banding and stress overshoot are not understood and under debate, therefore in-depth single-molecule studies of DNA are necessary to resolve remaining issues in polymer rheology.[11] These examinations at the single-molecule level will allow us to create new models, by unraveling the detailed molecular mechanisms behind various nonlinear rheology phenomena.

The field of DNA confinement has grown tremendously over the past decade, branching out into several directions ranging from DNA sequencing, separation, to DNA transfection. In the near future, the horizon of this field will be expanded allowing to study various crucial biological processes such as DNA translocation through nanopores (e.g., nuclear pore complexes),

transport of messenger RNA, and DNA–membrane interaction. We just found basic applications of nanofluidics for DNA analysis. Finally, we envision that nanofluidic systems will become a prominent platform to manipulate single cells and DNA, will provide effective tools for analyzing single biomolecules extracted from single cells and enable precise delivery of DNA into living cells. Despite several challenges, we expect that micro/nanofluidic community will actively continue to work on the development and applications of single-cell genomics, proteomics, metabolomics, and transcriptomics, by methodically increasing the complexity of nanofluidics experiments.

ACKNOWLEDGMENTS

[1] *Polymeric Biomaterials*, edited by S. Dumitriu and V. I. Popa (CRC Press, Taylor & Francis Group, Boca Raton, 2013).
[2] R. Pecora, Science **251**, 893 (1991).
[3] R. A. Hughes, A. E. Miklos, and A. D. Ellington, in *Methods Enzymol.*, edited by C. Voigt (Academic Press, 2011), pp. 277–309.
[4] P. J. Hagerman, Annu. Rev. Biophys. Biophys. Chem. **17**, 265 (1988).
[5] G. M. Whitesides, Nature **442**, 368 (2006).
[6] T. A. Waigh, Rep. Prog. Phys. **79**, 74601 (2016).
[7] S. R. Quake, Science **290**, 1536 (2000).
[8] D. Mijatovic, J. C. T. Eijkel, and A. van den Berg, Lab Chip **5**, 492 (2005).
[9] D. Qin, Y. Xia, and G. M. Whitesides, Nat. Protocol **5**, 491 (2010).
[10] Y. Lu, L. An, S.-Q. Wang, and Z.-G. Wang, ACS Macro Lett. **3**, 569 (2014).
[11] S.-Q. Wang, Soft Matter **11**, 1454 (2015).
[12] S. G. Hatzikiriakos and K. B. Migler, *Polymer Processing Instabilities: Control and Understanding* (CRC Press, 2004).
[13] G. G. Fuller, *Optical Rheometry of Complex Fluids* (Oxford University Press, New York, 1995).
[14] R. G. Larson, *The Structure and Rheology of Complex Fluids* (Oxford University Press, New York, 1999).
[15] T. J. Ober, S. J. Haward, C. J. Pipe, J. Soulages, and G. H. McKinley, Rheol. Acta **52**, 529 (2013).
[16] D. J. Mai, C. Brockman, and C. M. Schroeder, Soft Matter **8**, 10560 (2012).
[17] P. E. Boukany, S.-Q. Wang, S. Ravindranath, and L. J. Lee, Soft Matter **11**, 8058 (2015).
[18] P. G. de Gennes, J. Chem. Phys. **55**, 572 (1971).
[19] R. G. Larson, Science **318**, 57 (2007).
[20] T. T. Perkins, D. E. Smith, and S. Chu, Science **276**, 2016 (1997).
[21] C. M. Schroeder, E. S. G. Shaqfeh, and S. Chu, Macromolecules **37**, 9242 (2004).
[22] F. Persson and J. O. Tegenfeldt, Chem. Soc. Rev. **39**, 985 (2010).
[23] S. L. Levy and H. G. Craighead, Chem. Soc. Rev. **39**, 1133 (2010).
[24] W. Reisner, J. N. Pedersen, and R. H. Austin, Rep. Prog. Phys. **75**, 106601 (2012).
[25] G. F. Schneider and C. Dekker, Nat. Biotechnol. **30**, 326 (2012).
[26] L. Bocquet and P. Tabeling, Lab. Chip **14**, 3143 (2014).
[27] R. Riehn, M. Lu, Y.-M. Wang, S. F. Lim, E. C. Cox, and R. H. Austin, Proc. Natl. Acad. Sci. U.S.A. **102**, 10012 (2005).
[28] W. Reisner, N. B. Larsen, A. Silahtaroglu, A. Kristensen, N. Tommerup, J. O. Tegenfeldt, and H. Flyvbjerg, Proc. Natl. Acad. Sci., U.S.A. **107**, 13294 (2010).
[29] J. McCaffrey, J. Sibert, B. Zhang, Y. Zhang, W. Hu, H. Riethman, and M. Xiao, Nucl. Acids Res. **44**, e11 (2016).
[30] S. L. Cockroft, J. Chu, M. Amorin, and M. R. Ghadiri, J. Am. Chem. Soc. **130**, 818 (2008).
[31] E. A. Manrao, I. M. Derrington, A. H. Laszlo, K. W. Langford, M. K. Hopper, N. Gillgren, M. Pavlenok, M. Niederweis, and J. H. Gundlach, Nat. Biotechnol. **30**, 349 (2012).
[32] J. Han and H. G. Craighead, Science **288**, 1026 (2000).
[33] R. Ashton, C. Padala, and R. S. Kane, Curr. Opin. Biotechnol. **14**, 497 (2003).
[34] T. Yasui, N. Kaji, R. Ogawa, S. Hashioka, M. Tokeshi, Y. Horiike, and Y. Baba, Anal. Chem. **83**, 6635 (2011).
[35] S. Wang and L. J. Lee, Biomicrofluidics **7**, 11301 (2013).
[36] P. W. Bridgman, *Dimensional Analysis* (Yale University Press, New Haven, 1963).
[37] *Dynamics of Polymeric Liquids*, edited by R. B. Bird, 2nd ed. (Wiley, New York, 1987).
[38] M. Reiner, Phys. Today **17**(1), 62 (1964).
[39] J. M. Dealy, Rheol. Bull. **79**, 14 (2010).
[40] L. E. Rodd, T. P. Scott, D. V. Boger, J. J. Cooper-White, and G. H. McKinley, J. Non-Newtonian Fluid Mech. **129**, 1 (2005).
[41] P. E. Arratia, C. C. Thomas, J. Diorio, and J. P. Gollub, Phys. Rev. Lett. **96**, 144502 (2006).
[42] Y. T. Hu, J. Rheol. **54**, 1307 (2010).
[43] S.-Q. Wang, S. Ravindranath, and P. Boukany, Macromolecules **44**, 183 (2011).
[44] H. S. Rye, J. M. Dabora, M. A. Quesada, R. A. Mathies, and A. N. Glazer, Anal. Biochem. **208**, 144 (1993).
[45] W. D. Volkmuth and R. H. Austin, Nature **358**, 600 (1992).
[46] W. D. Volkmuth, T. Duke, M. C. Wu, R. H. Austin, and A. Szabo, Phys. Rev. Lett. **72**, 2117 (1994).
[47] O. L. Hemminger, P. E. Boukany, S.-Q. Wang, and L. Lee, J. Non-Newtonian Fluid Mech. **165**, 1613 (2010).
[48] N. François, D. Lasne, Y. Amarouchene, B. Lounis, and H. Kellay, Phys. Rev. Lett. **100**, 18302 (2008).

[49]H. Aoki, K. Mori, and S. Ito, Soft Matter **8**, 4390 (2012).

[50]J. Tai, C. P. Lim, and Y. C. Lam, Sci. Rep. **5**, 16633 (2015).

[51]M. Keshavarz, H. Engelkamp, J. Xu, E. Braeken, M. B. J. Otten, H. Uji-i, E. Schwartz, M. Koepf, A. Vananroye, J. Vermant, R. J. M. Nolte, F. De Schryver, J. C. Maan, J. Hofkens, P. C. M. Christianen, and A. E. Rowan, ACS Nano **10**, 1434 (2016).

[52]K. Gunther, M. Mertig, and R. Seidel, Nucl. Acids Res. **38**, 6526 (2010).

[53]B. Kundukad, J. Yan, and P. S. Doyle, Soft Matter **10**, 9721 (2014).

[54]E. S. G. Shaqfeh, J. Non-Newtonian Fluid Mech. **130**, 1 (2005).

[55]*Rheology: Principles, Measurements, and Applications*, edited by C. W. Macosko (VCH, New York, 1994).

[56]T. T. Perkins, Quake, D. E. Smith, and S. Chu, Science **264**, 822 (1994).

[57]T. T. Perkins, D. E. Smith, and S. Chu, Science **264**, 819 (1994).

[58]B. H. Zimm, J. Chem. Phys. **24**, 269 (1956).

[59]P. Debye and A. M. Bueche, J. Chem. Phys. **16**, 573 (1948).

[60]M. Adam and M. Delsanti, Macromolecules **10**, 1229 (1977).

[61]A. Keller and J. Odell, Colloid Polym. Sci. **263**, 181 (1985).

[62]P. G. de Gennes, *Scaling Concepts in Polymer Physics* (Cornell University Press, Ithaca, N. Y, 1979).

[63]D. R. Tree, A. Muralidhar, P. S. Doyle, and K. D. Dorfman, Macromolecules **46**, 8369 (2013).

[64]M. Doi and S. F. Edwards, *The Theory of Polymer Dynamics* (Oxford University Press, 1988).

[65]D. E. Smith, T. T. Perkins, and S. Chu, Phys. Rev. Lett. **75**, 4146 (1995).

[66]R. E. Teixeira, A. K. Dambal, D. H. Richter, E. S. Shaqfeh, and S. Chu, Macromolecules **40**, 2461 (2007).

[67]K.-W. Hsiao, C. Samsal, J. R. Prakash, and C. M. Schroeder, e-print arXiv.org/abs/1604.06754 Cond-Mat.

[68]Y. Li, K.-W. Hsiao, C. A. Brockman, D. Y. Yates, R. M. Robertson-Anderson, J. A. Kornfield, M. J. San Francisco, C. M. Schroeder, and G. B. McKenna, Macromolecules **48**, 5997 (2015).

[69]D. J. Mai, A. B. Marciel, C. E. Sing, and C. M. Schroeder, ACS Macro Lett. **4**, 446 (2015).

[70]A. B. Marciel, D. J. Mai, and C. M. Schroeder, Macromolecules **48**, 1296 (2015).

[71]P. G. de Gennes, J. Chem. Phys. **60**, 5030 (1974).

[72]R. G. Larson and J. J. Magda, Macromolecules **22**, 3004 (1989).

[73]D. E. Smith and S. Chu, Science **281**, 1335 (1998).

[74]C. M. Schroeder, H. P. Babcock, E. S. G. Shaqfeh, and S. Chu, Science **301**, 1515 (2003).

[75]R. G. Larson, H. Hu, D. E. Smith, and S. Chu, J. Rheol. **43**, 267 (1999).

[76]P. G. de Gennes, Science **276**, 1999 (1997).

[77]D. E. Smith, H. P. Babcock, and S. Chu, Science **283**, 1724 (1999).

[78]C. M. Schroeder, R. E. Teixeira, E. S. G. Shaqfeh, and S. Chu, Phys. Rev. Lett. **95**, 18301 (2005).

[79]J. S. Hur, E. S. G. Shaqfeh, H. P. Babcock, D. E. Smith, and S. Chu, J. Rheol. **45**, 421 (2001).

[80]P. E. Boukany, O. Hemminger, S.-Q. Wang, and L. Lee, Phys. Rev. Lett. **105**, 27802 (2010).

[81]S. Gulati, S. J. Muller, and D. Liepmann, Biomicrofluidics **9**, 54102 (2015).

[82]D. V. Boger, Annu. Rev. Fluid Mech. **19**, 157 (1987).

[83]F. P. T. Baaijens, J. Non-Newtonian Fluid Mech. **79**, 361 (1998).

[84]S. A. White, A. D. Gotsis, and D. G. Baird, J. Non-Newtonian Fluid Mech. **24**, 121 (1987).

[85]A. Groisman and V. Steinberg, Nature **405**, 53 (2000).

[86]S. Gerashchenko, C. Chevallard, and V. Steinberg, EPL **71**, 221 (2005).

[87]G. Boffetta, A. Celani, and S. Musacchio, Phys. Rev. Lett. **91**, 34501 (2003).

[88]Y. Liu and V. Steinberg, in *Macromol. Symp.* (Wiley Online Library, 2014), pp. 34–43.

[89]H. Bodiguel, J. Beaumont, A. Machado, L. Martinie, H. Kellay, and A. Colin, Phys. Rev. Lett. **114**, 28302 (2015).

[90]L. Pan, A. Morozov, C. Wagner, and P. Arratia, Phys. Rev. Lett. **110**, 174502 (2013).

[91]B. Meulenbroek, C. Storm, V. Bertola, C. Wagner, D. Bonn, and W. van Saarloos, Phys. Rev. Lett. **90**, 24502 (2003).

[92]V. Bertola, B. Meulenbroek, C. Wagner, C. Storm, A. Morozov, W. van Saarloos, and D. Bonn, Phys. Rev. Lett. **90**, 114502 (2003).

[93]A. N. Morozov and W. van Saarloos, Phys. Rev. Lett. **95**, 24501 (2005).

[94]F. Latinwo and C. M. Schroeder, Soft Matter **10**, 2178 (2014).

[95]C. Bustamante, Z. Bryant, and S. B. Smith, Nature **421**, 423 (2003).

[96]D. Bonn, Y. Amarouchène, C. Wagner, S. Douady, and O. Cadot, J. Phys. Condens. Matter **17**, S1195 (2005).

[97]M. Tabor and P. G. de Gennes, EPL **2**, 519 (1986).

[98]K. R. Sreenivasan and C. M. White, J. Fluid Mech. **409**, 149 (2000).

[99]Y. Amarouchene, D. Bonn, H. Kellay, T.-S. Lo, V. S. L'vov, and I. Procaccia, Phys. Fluids **20**, 65108 (2008).

[100]N. François, Y. Amarouchene, B. Lounis, and H. Kellay, EPL **86**, 34002 (2009).

[101]W.-C. Liao, X. Hu, W. Wang, and L. J. Lee, Biomicrofluidics **7**, 34103 (2013).

[102]X. Michalet, R. Ekong, F. Fougerousse, S. Rousseaux, C. Schurra, N. Hornigold, M. van Slegtenhorst, J. Wolfe, S. Povey, J. S. Beckmann, and A. Bensimon, Science **277**, 1518 (1997).

[103]J. Guan, N. Ferrell, B. Yu, D. J. Hansford, and L. J. Lee, Soft Matter **3**, 1369 (2007).

[104]J. Guan, B. Yu, and L. J. Lee, Adv. Mater. **19**, 1212 (2007).

[105]J. Guan and L. J. Lee, Proc. Natl. Acad. Sci. U. S. A. **102**, 18321 (2005).

[106]P. J. Glazer, L. Bergen, L. Jennings, A. J. Houtepen, E. Mendes, and P. E. Boukany, Small **10**, 1729 (2014).

[107]J. Guan, P. E. Boukany, O. Hemminger, N.-R. Chiou, W. Zha, M. Cavanaugh, and L. J. Lee, Adv. Mater. **22**, 3997 (2010).

[108]M. Muthukumar, Annu. Rev. Biophys. Biomol. Struct. **36**, 435 (2007).

[109]C. Dekker, Nat. Nanotechnol. **2**, 209 (2007).

[110]D. Wang and S. Bodovitz, Trends Biotechnol. **28**, 281 (2010).

[111]N. Kaji, Y. Okamoto, M. Tokeshi, and Y. Baba, Chem. Soc. Rev. **39**, 948 (2010).

[112]J. Xuan and M. L. Lee, Anal. Methods **6**, 27 (2014).

[113]T. Yasui, N. Kaji, and Y. Baba, Annu. Rev. Anal. Chem. **6**, 83 (2013).

[114]D. G. Haywood, A. Saha-Shah, L. A. Baker, and S. C. Jacobson, Anal. Chem. **87**, 172 (2015).

[115]D. J. Bonthuis, C. Meyer, D. Stein, and C. Dekker, Phys. Rev. Lett. **101**, 108303 (2008).

[116]W. Reisner, K. J. Morton, R. Riehn, Y. M. Wang, Z. Yu, M. Rosen, J. C. Sturm, S. Y. Chou, E. Frey, and R. H. Austin, Phys. Rev. Lett. **94**, 196101 (2005).

[117]C.-C. Hsieh and P. S. Doyle, Korea-Aust. Rheol. J. **20**, 127 (2008).

[118]L. Dai, C. B. Renner, and P. S. Doyle, Adv. Colloid Interface Sci. **232**, 80 (2016).

[119]P. Pincus, Macromolecules **9**, 386 (1976).

[120]M. Rubinstein and R. H. Colby, *Polymer Physics* (Oxford University Press, Oxford, New York, 2003).

[121]T. Odijk, Macromolecules **16**, 1340 (1983).

[122]M. Daoud and P. G. de Gennes, J. Phys. **38**, 85 (1977).

[123]Y. Yang, T. W. Burkhardt, and G. Gompper, Phys. Rev. E **76**, 11804 (2007).

[124]Y. Wang, D. R. Tree, and K. D. Dorfman, Macromolecules **44**, 6594 (2011).

[125]T. Odijk, Phys. Rev. E **77**, 60901 (2008).

[126]L. Dai, J. van der Maarel, and P. S. Doyle, Macromolecules **47**, 2445 (2014).

[127]L. Dai and P. S. Doyle, Macromolecules **46**, 6336 (2013).

[128]E. Werner and B. Mehlig, Phys. Rev. E **90**, 62602 (2014).

[129]W. Reisner, J. P. Beech, N. B. Larsen, H. Flyvbjerg, A. Kristensen, and J. O. Tegenfeldt, Phys. Rev. Lett. **99**, 58302 (2007).

[130]C.-C. Hsieh, A. Balducci, and P. S. Doyle, Nano Lett. **8**, 1683 (2008).

[131]J. Lee, S. Kim, H. Jeong, G. Y. Jung, R. Chang, Y.-L. Chen, and K. Jo, ACS Macro Lett. **3**, 926 (2014).

[132]C. Zhang, P. G. Shao, J. A. van Kan, and J. R. C. van der Maarel, Proc. Natl. Acad. Sci., U.S.A **106**, 16651 (2009).

[133]J. J. Jones, J. R. C. van der Maarel, and P. S. Doyle, Nano Lett. **11**, 5047 (2011).

[134]R. Marie and A. Kristensen, J. Biophotonics **5**, 673 (2012).

[135]D. Xia, J. Yan, and S. Hou, Small **8**, 2787 (2012).

[136]A. C. Y. Mak, Y. Y. Y. Lai, E. T. Lam, T.-P. Kwok, A. K. Y. Leung, A. Poon, Y. Mostovoy, A. R. Hastie, W. Stedman, T. Anantharaman, W. Andrews, X. Zhou, A. W. C. Pang, H. Dai, C. Chu, C. Lin, J. J. K. Wu, C. M. L. Li, J.-W. Li, A. K. Y. Yim, S. Chan, J. Sibert, Ž. Džakula, H. Cao, S.-M. Yiu, T.-F. Chan, K. Y. Yip, M. Xiao, and P.-Y. Kwok, Genetics **202**, 351 (2016).

[137]R. Marie, J. N. Pedersen, D. L. V. Bauer, K. H. Rasmussen, M. Yusuf, E. Volpi, H. Flyvbjerg, A. Kristensen, and K. U. Mir, Proc. Natl. Acad. Sci., U.S.A. **110**, 4893 (2013).

[138]K. T. Sørensen, J. M. Lopacinska, N. Tommerup, A. Silahtaroglu, A. Kristensen, and R. Marie, Rev. Sci. Instrum. **86**, 63702 (2015).

[139]Y. Kim, K. Seok Kim, K. L. Kounovsky, R. Chang, G. Young Jung, J. J. dePablo, K. Jo, and D. C. Schwartz, Lab Chip **11**, 1721 (2011).

[140]D. Stein, F. H. J. van der Heyden, W. J. A. Koopmans, and C. Dekker, Proc. Natl. Acad. Sci., U.S.A. **103**, 15853 (2006).

[141]X. Wang, L. Liu, Q. Pu, Z. Zhu, G. Guo, H. Zhong, and S. Liu, J. Am. Chem. Soc. **134**, 7400 (2012).

[142]X. Wang, V. Veerappan, C. Cheng, X. Jiang, R. D. Allen, P. K. Dasgupta, and S. Liu, J. Am. Chem. Soc. **132**, 40 (2010).

[143]L. Liu, V. Veerappan, Q. Pu, C. Cheng, X. Wang, L. Lu, R. D. Allen, and G. Guo, Anal. Chem. **86**, 729 (2014).

[144]K. D. Dorfman, S. B. King, D. W. Olson, J. D. P. Thomas, and D. R. Tree, Chem. Rev. **113**, 2584 (2013).

[145]C. Gupta, W.-C. Liao, D. Gallego-Perez, C. E. Castro, and L. J. Lee, Biomicrofluidics **8**, 24114 (2014).

[146]J. T. Mannion, C. H. Reccius, J. D. Cross, and H. G. Craighead, Biophys. J. **90**, 4538 (2006).

[147]S. L. Levy, J. T. Mannion, J. Cheng, C. H. Reccius, and H. G. Craighead, Nano Lett. **8**, 3839 (2008).

[148]W. Reisner, N. B. Larsen, H. Flyvbjerg, J. O. Tegenfeldt, and A. Kristensen, Proc. Natl. Acad. Sci., U.S.A. **106**, 79 (2009).

[149]M. B. Mikkelsen, W. Reisner, H. Flyvbjerg, and A. Kristensen, Nano Lett. **11**, 1598 (2011).

[150]C. R. Martin and Z. S. Siwy, Science **317**, 331 (2007).

[151]J. J. Kasianowicz, J. W. F. Robertson, E. R. Chan, J. E. Reiner, and V. M. Stanford, Annu. Rev. Anal. Chem. **1**, 737 (2008).

[152]S. Howorka and Z. Siwy, Chem. Soc. Rev. **38**, 2360 (2009).

[153]J. E. Reiner, A. Balijepalli, J. W. F. Robertson, J. Campbell, J. Suehle, and J. J. Kasianowicz, Chem. Rev. **112**, 6431 (2012).

[154]G. Wang, L. Wang, Y. Han, S. Zhou, and X. Guan, Acc. Chem. Res. **46**, 2867 (2013).

[155]W. H. Coulter, Patent No. 2656508 (20 October 1953).

[156]J. K. Rosenstein, M. Wanunu, C. A. Merchant, M. Drndic, and K. L. Shepard, Nat. Methods **9**, 487 (2012).

[157]C. Plesa and C. Dekker, Nanotechnology **26**, 84003 (2015).

[158]R. M. M. Smeets, U. F. Keyser, D. Krapf, M.-Y. Wu, N. H. Dekker, and C. Dekker, Nano Lett. **6**, 89 (2006).

[159]H. Chang, B. M. Venkatesan, S. M. Iqbal, G. Andreadakis, F. Kosari, G. Vasmatzis, D. Peroulis, and R. Bashir, Biomed. Microdevices **8**, 263 (2006).

[160]S. W. Kowalczyk and C. Dekker, Nano Lett. **12**, 4159 (2012).

[161]B. Luan and G. Stolovitzky, Nanotechnology **24**, 195702 (2013).

[162]K. Chen, L. Shan, S. He, G. Hu, Y. Meng, and Y. Tian, J. Phys. Chem. C **119**, 8329 (2015).

[163]D. Panja, G. T. Barkema, and A. B. Kolomeisky, J. Phys. Condens. Matter **25**, 413101 (2013).

[164]M. Wanunu, Phys. Life Rev. **9**, 125 (2012).

[165]S. E. Henrickson, M. Misakian, B. Robertson, and J. J. Kasianowicz, Phys. Rev. Lett. **85**, 3057 (2000).

[166]M. Wanunu, J. Sutin, B. McNally, A. Chow, and A. Meller, Biophys. J. **95**, 4716 (2008).

[167]M. Wanunu, W. Morrison, Y. Rabin, A. Y. Grosberg, and A. Meller, Nat. Nanotechnol. **5**, 160 (2010).

[168]H. Wang, J. E. Dunning, A. P.-H. Huang, J. A. Nyamwanda, and D. Branton, Proc. Natl. Acad. Sci. U.S.A. **101**, 13472 (2004).

[169]O. K. Dudko, J. Mathé, A. Szabo, A. Meller, and G. Hummer, Biophys. J. **92**, 4188 (2007).

[170]Q. Jin, A. M. Fleming, C. J. Burrows, and H. S. White, J. Am. Chem. Soc. **134**, 11006 (2012).

[171]A. Stachiewicz and A. Molski, J. Comput. Chem. **37**, 467 (2016).

[172]S. Benner, R. J. A. Chen, N. A. Wilson, R. Abu-Shumays, N. Hurt, K. R. Lieberman, D. W. Deamer, W. B. Dunbar, and M. Akeson, Nat. Nanotechnol. **2**, 718 (2007).

[173]B. Hornblower, A. Coombs, R. D. Whitaker, A. Kolomeisky, S. J. Picone, A. Meller, and M. Akeson, Nat. Methods **4**, 315 (2007).

[174]B. M. Venkatesan and R. Bashir, Nat. Nanotechnol. **6**, 615 (2011).

[175]M. Muthukumar, C. Plesa, and C. Dekker, Phys. Today **68**(8), 40 (2015).

[176]U. F. Keyser, Nat. Nanotechnol. **11**, 106 (2016).

[177]J. J. Kasianowicz, E. Brandin, D. Branton, and D. W. Deamer, Proc. Natl. Acad. Sci., U.S.A. **93**, 13770 (1996).

[178]Y. Feng, Y. Zhang, C. Ying, D. Wang, and C. Du, Genom. Proteom. Bioinform. **13**, 4 (2015).

[179]J. Kudr, S. Skalickova, L. Nejdl, A. Moulick, B. Ruttkay–Nedecky, V. Adam, and R. Kizek, Electrophoresis **36**, 2367 (2015).

[180]S. Hernández-Ainsa, N. A. W. Bell, V. V. Thacker, K. Göpfrich, K. Misiunas, M. E. Fuentes-Perez, F. Moreno-Herrero, and U. F. Keyser, ACS Nano **7**, 6024 (2013).

[181]S. Hernández-Ainsa and U. F. Keyser, Nanoscale **6**, 14121 (2014).

[182]Y. Zhang, G. Wu, W. Si, J. Sha, L. Liu, and Y. Chen, Chin. Sci. Bull. **59**, 4908 (2014).

[183]K. Venta, G. Shemer, M. Puster, J. A. Rodríguez-Manzo, A. Balan, J. K. Rosenstein, K. Shepard, and M. Drndić, ACS Nano **7**, 4629 (2013).

[184]S. Banerjee, J. Wilson, J. Shim, M. Shankla, E. A. Corbin, A. Aksimentiev, and R. Bashir, Adv. Funct. Mater. **25**, 936 (2015).

[185]Z. Gu, Y. Zhang, B. Luan, and R. Zhou, Soft Matter **12**, 817 (2016).

[186]J. Feng, K. Liu, R. D. Bulushev, S. Khlybov, D. Dumcenco, A. Kis, and A. Radenovic, Nat. Nanotechnol. **10**, 1070 (2015).

[187]A. H. Laszlo, I. M. Derrington, B. C. Ross, H. Brinkerhoff, A. Adey, I. C. Nova, J. M. Craig, K. W. Langford, J. M. Samson, R. Daza, K. Doering, J. Shendure, and J. H. Gundlach, Nat. Biotechnol. **32**, 829 (2014).

[188]S. Carson, J. Wilson, A. Aksimentiev, and M. Wanunu, Biophys. J. **107**, 2381 (2014).

[189]B. Lu, F. Albertorio, D. P. Hoogerheide, and J. A. Golovchenko, Biophys. J. **101**, 70 (2011).

[190]C. Plesa, N. van Loo, P. Ketterer, H. Dietz, and C. Dekker, Nano Lett. **15**, 732 (2015).

[191]S. Carson and M. Wanunu, Nanotechnology **26**, 74004 (2015).

[192]G. M. Cherf, K. R. Lieberman, H. Rashid, C. E. Lam, K. Karplus, and M. Akeson, Nat. Biotechnol. **30**, 344 (2012).

[193]U. F. Keyser, B. N. Koeleman, S. van Dorp, D. Krapf, R. M. M. Smeets, S. G. Lemay, N. H. Dekker, and C. Dekker, Nat. Phys. **2**, 473 (2006).

[194]H. Peng and X. S. Ling, Nanotechnology **20**, 185101 (2009).

[195]V. Lulevich, S. Kim, C. P. Grigoropoulos, and A. Noy, Nano Lett. **11**, 1171 (2011).

[196]B. Lu, D. P. Hoogerheide, Q. Zhao, H. Zhang, Z. Tang, D. Yu, and J. A. Golovchenko, Nano Lett. **13**, 3048 (2013).

[197]H. Zhang, Q. Zhao, Z. Tang, S. Liu, Q. Li, Z. Fan, F. Yang, L. You, X. Li, J. Zhang, and D. Yu, Small **9**, 4112 (2013).

[198]Y. He, M. Tsutsui, C. Fan, M. Taniguchi, and T. Kawai, ACS Nano **5**, 5509 (2011).

[199]Z. Tang, Z. Liang, B. Lu, J. Li, R. Hu, Q. Zhao, and D. Yu, Nanoscale **7**, 13207 (2015).

[200]H. Bayley, Clin. Chem. **61**, 25 (2015).

[201]S. Huang, M. Romero-Ruiz, O. K. Castell, H. Bayley, and M. I. Wallace, Nat. Nanotechnol. **10**, 986 (2015).

[202]M. L. Yarmush, A. Golberg, G. Serša, T. Kotnik, and D. Miklavčič, Annu. Rev. Biomed. Eng. **16**, 295 (2014).

[203]L. Lambricht, A. Lopes, Š. Kos, G. Serša, V. Préat, and G. Vandermeulen, Expert Opin. Drug Deliv. **13**, 295 (2016).

[204]J. C. Weaver and Y. A. Chizmadzhev, Bioelectrochem. Bioenerg. **41**, 135 (1996).

[205]P. T. Vernier, Z. A. Levine, and M. A. Gundersen, Proc. IEEE **101**, 494 (2013).

[206]R. Benz and U. Zimmermann, Biochim. Biophys. Acta BBA - Biomembr. **640**, 169 (1981).

[207]Z. A. Levine and P. T. Vernier, J. Membr. Biol. **236**, 27 (2010).

[208]M. Szabo and M. I. Wallace, Biochim. Biophys. Acta BBA - Biomembr. **1858**, 613 (2016).

[209]M. Golzio, J. Teissié, and M.-P. Rols, Proc. Natl. Acad. Sci., U.S.A. **99**, 1292 (2002).

[210]C. Rosazza, E. Phez, J.-M. Escoffre, L. Cézanne, A. Zumbusch, and M.-P. Rols, Int. J. Pharm. **423**, 134 (2012).

[211]B. Markelc, E. Skvarca, T. Dolinsek, V. P. Kloboves, A. Coer, G. Sersa, and M. Cemazar, Bioelectrochemistry **103**, 111 (2015).

[212]P. E. Boukany, A. Morss, W. Liao, B. Henslee, H. Jung, X. Zhang, B. Yu, X. Wang, Y. Wu, L. Li, K. Gao, X. Hu, X. Zhao, O. Hemminger, W. Lu, G. P. Lafyatis, and L. J. Lee, Nat. Nanotechnol. **6**, 747 (2011).

[213]X. Xie, A. M. Xu, S. Leal-Ortiz, Y. Cao, C. C. Garner, and N. A. Melosh, ACS Nano **7**, 4351 (2013).

[214]D. Bonn, F. Ingremeau, Y. Amarouchene, and H. Kellay, Phys. Rev. E **84**, 045301 (2011).